

Digital-Twin-Aided Dynamic Spectrum Sharing and Resource Management in Integrated Satellite-Terrestrial Networks

Hung Nguyen-Kha[✉], *Graduate Student Member, IEEE*, Vu Nguyen Ha[✉], *Senior Member, IEEE*, Ti Nguyen[✉], *Member, IEEE*, Eva Lagunas[✉], *Senior Member, IEEE*, Joel Grotz[✉], *Senior Member, IEEE*, Symeon Chatzinotas[✉], *Fellow, IEEE*, and Björn Ottersten[✉], *Fellow, IEEE*

Abstract—The explosive growth in wireless service demand has prompted the evolution of integrated satellite-terrestrial networks (ISTNs) to overcome the limitations of traditional terrestrial networks (TNs) in terms of coverage, spectrum efficiency, and deployment cost. Particularly, leveraging LEO satellites and dynamic spectrum sharing (DSS), ISTNs offer promising solutions but face significant challenges due to diverse terrestrial environments, user and satellite mobility, and long propagation LEO-to-ground distance. To address these challenges, digital-twin (DT) has emerged as a promising technology to offer virtual replicas of real-world systems, facilitating prediction for resource management. In this work, we study a time-window-based DT-aided DSS framework for ISTNs, enabling joint long-term and short-term resource decisions to reduce system congestion. Based on that, two optimization problems are formulated, which aim to optimize resource management using DT information and to refine obtained solutions with actual real-time information, respectively. To efficiently solve these problems, we proposed algorithms using compressed-sensing-based and successive convex approximation techniques. Simulation results using actual traffic data and the London 3D map demonstrate the superiority in terms of congestion minimization of our proposed algorithms compared to benchmarks. Additionally, it shows the adaptation ability and practical feasibility of our proposed solutions.

Index Terms—LEO, ISTNs, C-Band, Digital Twin, 5G-NR, Resource Allocation.

I. INTRODUCTION

In recent years, the explosive growth in mobile traffic and emerging service demands, such as seamless and ubiquitous connectivity, have driven the evolution of wireless communication. While next-generation (NextG) networks are envisioned to meet these requirements [2], [3], relying solely on denser TN deployment faces significant challenges, including inefficient spectrum utilization in sparsely populated areas and high infrastructure costs. To overcome these limitations, non-terrestrial networks (NTNs), notably satellite networks (SatNet), can offer complementary coverage and traffic offloading. Leveraging both TN and SatNet capabilities, ISTNs have attracted much attention as a viable architecture to meet NextG requirements, advancing the goal of global, uninterrupted coverage. Backed by regulatory and institutional bodies such as the US Federal Communications Commission (FCC) and the European Space Agency (ESA), ISTNs are

This work was supported by the Luxembourg National Research Fund (FNR) under the project INSTRUCT (IPBG19/14016225/INSTRUCT). The preliminary result of this manuscript is presented in IEEE GLOBECOM'25 [1]. H. Nguyen-Kha, V. N. Ha, T. Nguyen, E. Lagunas, S. Chatzinotas, B. Ottersten are with the Interdisciplinary Centre for Security, Reliability and Trust (SnT), University of Luxembourg, 1855 Luxembourg Ville, Luxembourg. (e-mail: {khahung.nguyen; vu.nguyen.ha; titi.nguyen; eva.lagunas; Symeon.Chatzinotas, bjorn.ottersten}@uni.lu). J. Grotz is with SES, Chateau de Betzdorf, Betzdorf 6815, Luxembourg (e-mail: Joel.Grotz@ses.com).

recognized as enablers of direct-to-device (D2D) connectivity and TN support [4], [5]. Among the SatNet options, low Earth orbit (LEO) satellites (LSats) offer lower latency and higher channel gain, making them especially suited for tight TN-NTN integration and native support of NTNs in 6G [3].

To realize ubiquitous connectivity in 6G with ISTNs, efficient use of radio spectrum across TNs and SatNets becomes critical. Traditionally, these two networks have operated in separate radio frequency bands (RFBs), with TNs utilizing lower bands and SatNet relying on higher ones. However, due to limited spectrum availability, this static allocation strategy poses limitations, especially in densely deployed or heterogeneous traffic environments. To address these constraints, dynamic spectrum sharing (DSS) between TNs and SatNets appears as an important strategy within ISTNs to improve spectral efficiency. Recent proposals, such as MediaTek's spectrum reuse framework, highlight the potential of allowing SatNet to opportunistically access terrestrial spectrum [6]. This vision is further reinforced by regulatory bodies like the FCC and ESA, which support co-primary spectrum use between TN and NTN systems, particularly for D2D connectivity [4], [5]. Nevertheless, enabling spectrum sharing in ISTNs introduces critical challenges, especially inter-system interference (ISyI) between coexisting TN and SatNet transmissions.

Effectively managing ISyI is essential to realize the full potential of DSS in 6G-ISTN architectures. This, however, demands advanced technologies to address key challenges stemming from the wide coverage areas, high mobility of LSats, and the long LSat-to-ground (Sat2G) distance. Moreover, LSats often serve regions with diverse terrestrial conditions, especially in urban areas, where dense buildings introduce reflection, diffraction, and signal blockage, further complicating interference patterns. In addition, the movement of both LSats and users leads to rapidly varying link conditions, while the long Sat2G increases the overhead for signaling and real-time channel estimation. To address these challenges, digital-twin (DT) has emerged as a promising technology to offer virtual replicas of real-world systems, which enables capturing and emulating the evolution of the physical environments, network dynamics, and entities in real time [7], [8] through continuous monitoring. In the context of ISTNs, utilizing DT to replicate traffic demand, environmental conditions [9], and channel state information (CSI) can significantly enhance resource management (RM), support proactive interference mitigation, and reduce Sat2G control signaling by using DT information. This work leverages DT to address the key challenges of ISyI, DSS coordination, and RM in practical ISTN deployments.

A. Related Works

Spectrum sharing (SS) designs in ISTNs have been considered in literature [10]–[16]. In [10]–[13], snapshot-based SS solutions for ISTNs were considered. In particular, [10] designed the second-price auction mechanism to achieve an equilibrium SS solution for TNs and SatNet-based traffic offloading. [11] considered a backhaul and access SS framework, where one satellite served both base stations (BSs) and users (UEs). Limited backhaul link capacity, the UE association, allocates bandwidth (BW) assignment, and power control were addressed through the corresponding sub-problems. [12] and [13] studied the RA problems for throughput maximization in reverse SS scenarios [12] and in underlay/overlay sharing cases [13]. However, these snapshot-based works have not considered ubiquitous and seamless connectivity and struggle to capture the dynamic behavior of ISTNs.

The time-window-based SS systems have been examined in [14]–[16]. Specifically, [14] studied DSS for ISTNs, where a centralized coordinator BW to each network based on traffic load. In [15], the TN spectrum was temporarily shared with SatNet. The study focused on beam management, scheduling, and DSS for only SatNet, while TNs were considered under interference constraints. Both [14], [15] have not considered interference and service requirements at the user side. Additionally, their designs mainly rely on the statistical channel model. Filling these gaps, our previous work [16] has utilized 3D map and the ray-tracing (RayT) mechanism to examine the seamless connectivity and coverage enhancement in urban areas. However, [16] did not consider BW and RB allocation.

Recently, the DT technology has been utilized in RM [17]–[22]. However, existing DT models are predominantly used to replicate the computation information [17]–[20], traffic/load patterns [18], [22], and node positions [18], [19], [21]. Besides, given the crucial role of CSI in wireless RM, [22] incorporated CSI into the DT model using the statistical channel. Nevertheless, CSI is strongly affected by the surrounding environment, particularly in complex areas such as urban scenarios [16], [23]. Therefore, modeling the environment and its influence on CSI is essential, and should be incorporated into DT frameworks using 3D maps and RayT mechanisms [9]. To the best of our knowledge, the joint design of BW allocation, traffic steering, AP/LSat-UE association, RB assignment, and power control in DSS ISTNs with DT-aided, incorporating a realistic channel model based on actual 3D maps, has not been thoroughly investigated. This motivates us to fill this research gap in this work. The comparison between our work and the literature is summarized in Table I.

B. Research Contributions

According to the discussed research gap as well as D2D scenarios driven by ESA and FCC, this work studies novel DT-aided DSS mechanisms for ISTNs supporting D2D connectivity, where TNs and SatNets share the same 5G-NR RFBs. Regarding uneven traffic demand among services and systems, the work aims to minimize system congestion by improving spectrum usage through DSS and RM under practical constraints. This work's main contributions are summarized as:

- We investigate the 5G-NR transmission model for ISTNs under a practical system architecture and develop a novel

DT model to replicate key components of the network. Beyond replicating traffic demand and terminal positions, as done in prior works, our model incorporates realistic terminal antenna patterns, an actual 3D map of the target area, and a RayT tool to accurately emulate LSat/TN access point (TAP)-to-UE CSIs.

- We formulate two resource-allocation (RA) optimization problems, “*joint-RA*” and “*refinement*”, which respectively rely on DT-predicted information and real-time system feedback, such as CSIs and traffic arrival. The joint-RA problem leverages DT-predicted information to optimize both long-term RA decisions (i.e., traffic steering and BW allocation across services and TN/SatNet systems) and preliminary estimated short-term RA decisions (i.e., TAP/LSat-UE association, RB assignment, and power control). The refinement problem adjusts the TN short-term decisions based on real-time feedback to align the DT-optimized strategy with current environmental conditions. Both problems are challenging due to non-convex constraints; notably, the joint-RA problem is formulated as a mixed-integer non-linear program (MINLP) and relies on predicted information.
- By leveraging the DT model for predictive information and applying compressed sensing and successive convex approximation (SCA) techniques, we propose two efficient solution methods, named DT-based joint RA and Real-time refinement algorithms (*DT-JointRA* and *RT-Refine*), that address the problems in alignment with the system architecture.
- For practical evaluation, we utilize a realistic 3D map of London, mobility of UEs such as vehicle UEs extracted from UE route in Google Navigator, and actual data traffic datasets. Numerical results demonstrate that our proposed algorithms significantly outperform benchmarks in minimizing queue lengths. Moreover, with DT-assisted prediction and pre-optimization in DT-JointRA, the RT-Refine scheme achieves fast convergence within a few iterations, highlighting the practical feasibility and efficiency of the proposed solutions.

The rest of this paper is organized as follows. Section II presents the system model and problem formulation. Section IV and V describe the proposed solutions, benchmarks, and complexity analysis, respectively. Section VI and VII provide numerical results and the conclusion.

II. 5G-NR AND DIGITAL TWIN SYSTEM MODEL

This paper considers a 5G-NR-based downlink transmission in an ISTN consisting of N TAPs and one LSat jointly serving K UEs, as depicted in Fig. 1. It is assumed that SatNet employs the FDD strategy to manage downlink (DL) and uplink (UL) transmissions in distinct RFBs, whereas TN operates under the TDD mechanism for allocating radio resources between DL and UL in the same RFB [24]. In this context, we focus on utilizing the RFB, denoted W^{tot} (Hz), which is assumedly accessible to TN for both DL and UL with TDD management as well as the SatNet DL transmission.

A. Services and DT-based Network Management

The system supports three types of UEs, each associated with a specific communication service: (i) Delay-sensitive (D),

TABLE I: Comparison of related works.

Works	Year	Mode	Resource/Network Management								Digital Twin Replication					Channel model	
			SS mode	PC	UA	RB/SC	QoS	Intra SI	Inter SI	BWA	T/L/C	T/L	Computing	Position	3D Env	CSI	
[10]	2018	Snapshot	Primary-secondary	x	x	/	x	x	/	x	x	x	x	x	x	x	Statistic
[11]	2022	Snapshot	Non-overlap	✓	✓	x	Rate	✓	✓	✓	x	x	x	x	x	x	Statistic
[12]	2023	Snapshot	Overlap, non-overlap	x	x	/	x	/	/	x	x	x	x	x	x	x	Statistic
[13]	2024	Snapshot	Primary-secondary	✓	x	x	Rate	✓	✓	x	x	x	x	x	x	x	Statistic
[14]	2023	Time window	Non-overlap	✓	x	x	x	x	x	✓	✓	x	x	x	x	x	Statistic
[15]	2024	Time window	Overlap	x	✓	x	x	✓	✓	x	✓	x	x	x	x	x	Statistic
[16]	2025	Time window	Co-primary	✓	✓	x	rate	x	✓	x	x	x	x	x	x	x	3D map-based
[17]	2022	Snapshot	None	✓	✓	x	Latency	✓	x	x	✓	x	x	x	x	x	Statistic
[18]	2022	Snapshot	None	x	x	x	x	x	x	x	✓	✓	✓	✓	x	x	None
[19]	2023	Snapshot	None	x	x	x	Latency	x	x	✓	✓	x	✓	x	x	x	Statistic
[20]	2025	Snapshot	None	x	✓	x	x	x	x	✓	✓	x	✓	x	x	x	Statistic
[21]	2025	Time window	None	x	✓	✓	Latency	✓	x	x	x	x	x	✓	x	x	Statistic
[22]	2025	Time window	None	x	✓	x	Rate/Latency	x	x	✓	✓	✓	x	x	x	✓	Statistic
Our work	Time window	Slice, co-primary	✓	✓	✓	Latency	✓	✓	✓	✓	✓	x	✓	✓	✓	✓	3D map-based

PC: Power control, UA: User association, RB/SC: Resource-block/Sub-channel assignment, Inter/Intra SI: Inter/Intra system interference, BWA: Bandwidth allocation, T/L/C: Traffic/Load/Computing-resource

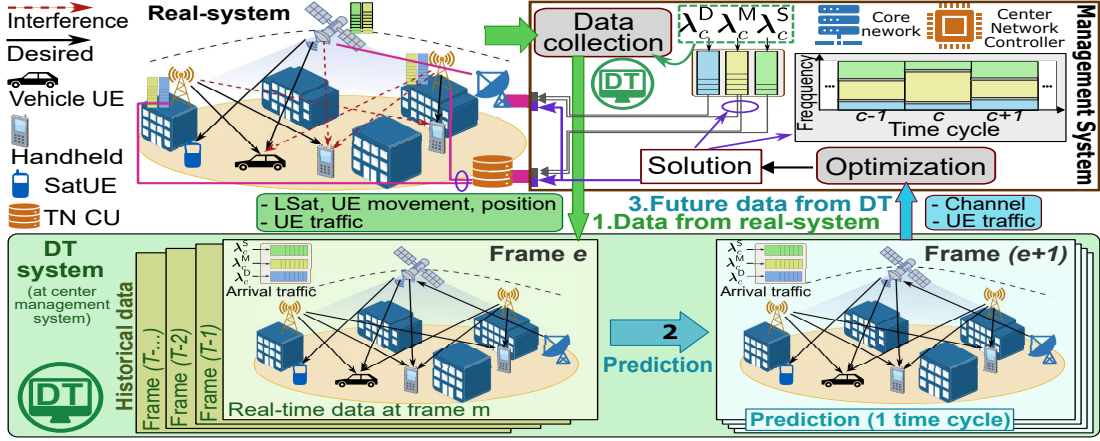
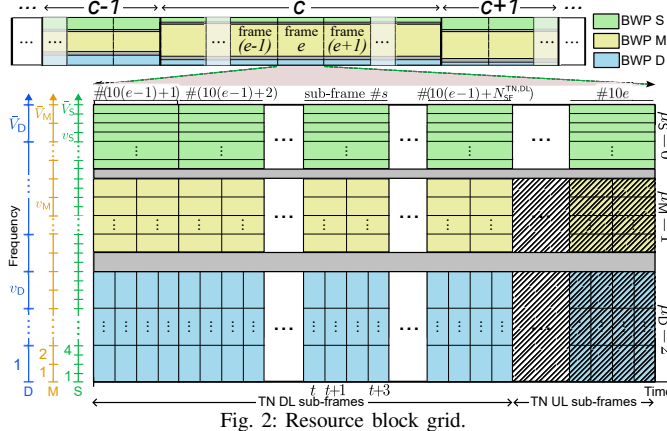


Fig. 1: Digital-twin-aided ISTNs.



such as uRLLC, exclusively served by TAPs; (ii) SatCom (S), provided solely by the LSat; and (iii) Multinet (M) supported by both TAPs and LSat. The sets of UEs associated with these three services are denoted as \mathcal{K}_D , \mathcal{K}_S , and \mathcal{K}_M , respectively. The total BW is dynamically divided into three BW parts (BWP) for these three services. Each BWP employs a 5G-NR numerology, i.e., μ_D , μ_M , and μ_S , tailored to its respective latency perspective. Let $\mathcal{K} = \mathcal{K}_D \cup \mathcal{K}_S \cup \mathcal{K}_M$, $\mathcal{L}, \mathcal{S}, L = |\mathcal{L}|$, $K_D = |\mathcal{K}_D|$, $K_S = |\mathcal{K}_S|$, and $K_M = |\mathcal{K}_M|$ be the sets of all UEs, TAPs, services, and numbers of TAPs and UEs. Hereafter, we denote \mathbf{AP}_ℓ and \mathbf{UE}_k the ℓ -th TAP and k -th UE.

As depicted in Fig. 1, this paper aims to jointly optimize “*long-term decisions*”, i.e., traffic steering from the core network (CN) to the LSat and TAPs, BW allocation (BWA) between TN and SatNet systems and across BWPs—executed at the central network management system (NMS)—as well as “*short-term decisions*”, i.e., UE association, RB assignment, and power control—executed at TN center unit (TCU) and gateway. To facilitate such optimization, we assume

the availability of a DT model with the virtual representation of network components to enable the prediction of network information. *The DT model will be presented in Section II-D.* The proposed optimization framework operates over multiple time scales, including cycle, frame, and sub-frame (SF), which will be detailed later.

This paper considers a time window of N_{CY} cycles. As depicted in Fig. 1, at the end of each cycle, the DT model updates its state **(1. Data from real-system)**, predicts **(2. Prediction)**, and provides predicted system-level information of the subsequent cycle to the NMS **(3. Future data from DT)**. Leveraging this foresight, the NMS performs joint resource management (**Optimization step**), generating long-term decisions along with preliminary estimates of short-term ones (at **Solution block**). This stage is referred as the “**DT-based Joint RA Stage**”. Each cycle is composed of multiple frames, with each frame consisting of 10 sub-frames (SFs). We assume that traffic rate information for D UEs can be updated at the SF level [25]. Hence, “*short-term decisions*” for the TN is further refined at the SF granularity (at TCU). This SF-level refinement process constitutes the “**RT-Refine Stage**”.

B. 5G-NR Standard-based Setting

1) *Frame and Sub-frame Setting*: According to 5G-NR standard, each frame duration is 10 ms ($T_{TF} = 10$ ms); hence, duration of one SF is 1 ms ($T_{SF} = 1$ ms). Assuming that each cycle c contains N_{TF} frames, the number of SFs in one cycle is $N_{SF} = 10N_{TF}$. Regarding the TDD transmission mode for TN, we assume that TN uses $N_{SF}^{TN,DL}$ beginning SFs for DL and $(10 - N_{SF}^{TN,DL})$ ending SFs for UL.

2) *Numerology Setting*: In this paper, numerologies used in BWPs are set as $\mu_S = 0$, $\mu_M = 1$ and $\mu_D = 2$, reflecting the increasing tolerance to delay across the three service types [26], [27]. Based on this, the RB grid is illustrated in Fig. 2.

a) *Time Domain*: Hereafter, we define the RB duration for service D as a *time slot* (TS) - the time unit. Based on that, the time indices RBs of service x n_x can be defined as

$$n_D = t, \quad n_M = \lceil t/2 \rceil, \quad n_S = \lceil t/4 \rceil, \quad (1)$$

respectively, where $\lceil \cdot \rceil$ is the ceil function. Furthermore, the RB duration of service x can be given as $T_x = 2^{-\mu_x}$ ms; hence, there are $N_x = 2^{\mu_x}$ RBs over one sub-channel of service x within a SF. Then, the time indices of cycles (c), frames (e), sub-frames (s) can be counted based on N_D as $c = \lceil t/(N_D N_{SF}) \rceil, e = \lceil t/(10N_D) \rceil, s = \lceil t/N_D \rceil$. In addition, the sets of RB indices in the time domain corresponding to service x within cycle c, frame e, and SF s can be defined as $\mathcal{T}_x^{\text{Cy},c} \triangleq \{(c-1)N_x N_{SF} + 1, \dots, cN_x N_{SF}\}, \mathcal{T}_x^{\text{TF},e} \triangleq \{(e-1)10N_x + 1, \dots, e10N_x\}$, and $\mathcal{T}_x^{\text{SF},s} \triangleq \{(s-1)N_x + 1, \dots, sN_x\}$.

b) *Frequency Domain*: Let $W_{x,c} = [f_{x,c}^{\min}, f_{x,c}^{\max}]$ be the frequency ranges of BWPs sliced for service x in cycle c. For simplicity, we set $f_{D,c}^{\max} \leq f_{M,c}^{\min}$ and $f_{M,c}^{\max} \leq f_{S,c}^{\min}$ for all c. Then, the BW of service x in cycle c is given as $W_{x,c} = f_{x,c}^{\max} - f_{x,c}^{\min}$. The BWPs are divided into sub-channels (SCs) due to various numerologies. For service x, the RB channel spacing is given as $w_x = 2^{\mu_x} \times 180$ kHz. Let $W^{\text{tot}} = f^{\max} - f^{\min}$ (Hz) denote the total BW. Then, the maximum SC number that can be assigned to the service x is $\bar{V}_x = \lfloor W^{\text{tot}}/w_x \rfloor$. We further denote v_x indices of the SCs in BWP x, and $\mathcal{V}_x \triangleq \{1, \dots, \bar{V}_x\}$, i.e., $v_x \in \mathcal{V}_x$. Once, the BWP of service x is defined, the SCs of \mathcal{V}_x located in the corresponding frequency range will be activated for service-x transmission. Hereafter, the RBs in BWP x are identified based on both time and frequency indices, i.e., $[v_x, n_x]$.

Following 5G standard, guard bands (GBs) between BWPs are considered. Here, the D-M separating GB BW should be half of w_D , i.e., $W_{G1} = f_{M,c}^{\min} - f_{D,c}^{\max} = w_D/2$, and the M-S separating GB BW is half of w_M , $W_{G2} = f_{S,c}^{\min} - f_{M,c}^{\max} = w_M/2$.

Remark 1. Denote $v_{D,c}^{\max}$ and $v_{M,c}^{\max}$ the maximum indices of activated SCs of service D and M in cycle c. With respect to GB, we can obtain $f_{M,c}^{\min} = f^{\min} + (2v_{D,c}^{\max} + 1)w_M = f^{\min} + (4v_{D,c}^{\max} + 2)w_S$ and $f_{S,c}^{\min} = f^{\min} + (2v_{M,c}^{\max} + 1)w_S$.

Let $\mathbf{b}_c \triangleq \{b_{v_x,c}^x \mid \forall v_x \in \mathcal{V}_x, x \in \mathcal{S}\}$ where $b_{v_x,c}^x = 1$ if SC v_x is activated in cycle c and $b_{v_x,c}^x = 0$ otherwise. Remark 1 yields,

$$(C1) : b_{v_D,c}^D + \sum_{i=1}^{2v_D+1} b_{i,c}^M + \sum_{j=1}^{4v_D+2} b_{j,c}^S \leq 1, \quad \forall (v_D, c),$$

$$(C2) : b_{v_M,c}^M + \sum_{j=1}^{2v_M+1} b_{j,c}^S \leq 1, \quad \forall (v_M, c).$$

Additionally, the system BW constraint yields

$$(C3) : \sum_{x \in \mathcal{S}} \sum_{v_x \in \mathcal{V}_x} b_{v_x,c}^x w_x + W_{G1} + W_{G2} \leq W^{\text{tot}}, \quad \forall c.$$

C. Channel Model

Let $\tilde{h}_{\ell,k}^{[v_x,n_x]}$ and $\tilde{g}_k^{[v_x,n_x]}$ be the channel coefficients of AP $_{\ell}$ -UE $_k$ and LSat-UE $_k$ links over RB $_{[v_x,n_x]}$, respectively. Omitting $[v_x, n_x]$, the channel coefficients are modeled as

$$\tilde{h}_{\ell,k} = \sqrt{PL_{\ell,k}} \left(\sqrt{\rho_{\ell,k}} \tilde{h}_{\ell,k}^{\text{ls}} + \sqrt{1 - \rho_{\ell,k}} \tilde{h}_{\ell,k}^{\text{nls}} \right), \quad (2)$$

$$\tilde{g}_k = \sqrt{PL_{0,k}} \left(\sqrt{\rho_{0,k}} \tilde{g}_k^{\text{ls}} + \sqrt{1 - \rho_{0,k}} \tilde{g}_k^{\text{nls}} \right), \quad (3)$$

based on the Rician model where $\rho_{\ell,k} = \tilde{K}_{\ell,k}/(\tilde{K}_{\ell,k} + 1)$; $\tilde{K}_{\ell,k}$, $PL_{\ell,k}$, $\tilde{h}_{\ell,k}$, $\tilde{h}_{\ell,k}^{\text{ls}}$, $\tilde{h}_{\ell,k}^{\text{nls}}$, $PL_{0,k}$, \tilde{g}_k^{ls} , and \tilde{g}_k^{nls} are the K-factor, path-loss, the corresponding line-of-sight (LoS) and non-line-of-sight (NLoS) components, respectively. In this work, we assume that TAPs can estimate perfectly CSIs for their served

UEs in each frame thanks to the pilot sent in TN uplink SFs [28]. The channel gain in cycle c and in frame e are denoted by $\{\mathbf{h}_c, \mathbf{g}_c\}$ and $\{\mathbf{h}_e, \mathbf{g}_e\}$. The relationship between the real-system and DT channels will be described in Section II-D4.

D. Digital-Twin Model

The DT system is deployed in NMS to replicate the environment and network components. As illustrated in Fig. 3, the DT model comprises a virtual system and computational functionalities. The virtual system consists of *static components*, including environmental features, TAP positions, and terminal antenna characteristics, as well as *dynamic components*, such as UE mobility, traffic demand, LSat movement, and CSIs. The DT model operation over each cycle is depicted in Fig. 1. Specifically, at the end of each cycle, the real mobility and traffic information are updated to the DT model. Using this information, computational functionalities are leveraged to emulate the real system's evolution in the next cycle and reflect it in the virtual one. The resulting predictions are then used in resource management for the subsequent cycle.

1) *Geographical Environment*: The DT system integrates 3D maps of the targeted areas. In cell ℓ , the corresponding environment in DT system is represented by

$$\widehat{\text{env}}_{\ell} = \{\text{map}_{\ell}\}, \quad \widehat{\text{AP}}_{\ell} = \{\mathbf{A}_{\ell}^{\text{ap}}, \mathbf{u}_{\ell}^{\text{ap}}\}, \quad \forall \ell \in \mathcal{L}, \quad (4)$$

wherein map_{ℓ} indicates the 3D map of the area in cell ℓ , $\mathbf{A}_{\ell}^{\text{ap}}$ and $\mathbf{u}_{\ell}^{\text{ap}}$ are the antenna properties and position of AP_{ℓ} .

2) *UE Information*: Virtual UE $_k$ in frame e is modeled as

$$\widehat{\text{UE}}_{k,[e]}^D = \{\mathbf{A}_k^{\text{ue}}, \hat{\mathbf{u}}_{k,[e]}^{\text{ue}}, \hat{\lambda}_{k,[s]}^{\text{SF},D} \mid_{s \in \mathcal{T}_{\text{SF}}^{\text{TF},e}}\}, \quad \forall k \in \mathcal{K}_D, \quad (5a)$$

$$\widehat{\text{UE}}_{k,[e]}^X = \{\mathbf{A}_k^{\text{ue}}, \hat{\mathbf{u}}_{k,[e]}^{\text{ue}}, \hat{\lambda}_{k,[e]}^{\text{TF},X}\}, \quad \forall k \in \mathcal{K}_X, X \in \{M, S\}, \quad (5b)$$

wherein $\mathcal{T}_{\text{SF}}^{\text{TF},e}$ is SF set in frame e, \mathbf{A}_k^{ue} , $\hat{\mathbf{u}}_{k,[e]}^{\text{ue}}$, $\hat{\lambda}_{k,[e]}^{\text{TF},X}$, and $\hat{\lambda}_{k,[s]}^{\text{SF},D}$ are the virtual antenna properties, position and traffic rate of UE $_k$ in frame e and SF s, respectively. The UE traffic rates will be described in Section III-E. This UE information in the upcoming cycle is obtained based on prediction techniques and updated information from the real environment.

3) *LSat Model*: The LSat DT at frame e is modeled as

$$\widehat{\text{Sat}}_{[e]} = \{\mathbf{A}^{\text{sat}}, \hat{\mathbf{u}}_{[e]}^{\text{sat}}, \text{TLE}_{[e]}\}, \quad (6)$$

where \mathbf{A}^{sat} , $\hat{\mathbf{u}}_{[e]}^{\text{sat}}$, and $\text{TLE}_{[e]}$ are the antenna properties, predicted position, and two-line-element (TLE) data of LSat in frame e, respectively. Due to the orbit stability and the frequent update framework, we assume that the LSat position is predicted with a negligible error, that is, $\hat{\mathbf{u}}_{[e]}^{\text{sat}} \approx \mathbf{u}_{[e]}^{\text{sat}}$.

4) *Channel Prediction*: Employing the RayT tool as in Fig. 3, the DT channel is identified as our previous work [16]

$$\text{chan}_{[e]} = \text{RT}(\widehat{\text{env}}_{\ell}, \widehat{\text{AP}}_{\ell}, \widehat{\text{Sat}}_{[e]}, \widehat{\text{UE}}_{k,[e]}), \quad (7)$$

where $\widehat{\text{UE}}_{k,[e]} = \{\widehat{\text{UE}}_{k,[e]}^X\}_{X \in \{M, S\}}, \text{chan}_{[e]} = \{\tilde{h}_{\ell,k}^{[\text{ls}, [v_x, n_x]}}, \tilde{h}_{\ell,k}^{[\text{nls}, [v_x, n_x]}}, \text{PL}_{\ell,k}^{[\text{ls}, [v_x, n_x]}}, \tilde{K}_{\ell,k}^{[\text{ls}, [v_x, n_x]}}, \tilde{g}_k^{[\text{ls}, [v_x, n_x]}}, \tilde{g}_k^{[\text{nls}, [v_x, n_x]}}, \text{PL}_{0,k}^{[\text{ls}, [v_x, n_x]}}, \tilde{K}_{0,k}^{[\text{ls}, [v_x, n_x]}\},$ with $\forall (\ell, k), \forall n_x \in \mathcal{T}_x^{\text{TF},e}$. In virtual environment, $\tilde{h}_{\ell,k}^{[\text{nls}, [v_x, n_x]}}$ and $\tilde{g}_k^{[\text{nls}, [v_x, n_x]}}$ are introduced to represent the NLoS components of DT channels. Those are different with $\tilde{h}_{\ell,k}^{[\text{ls}, [v_x, n_x]}}$ and $\tilde{g}_k^{[\text{ls}, [v_x, n_x]}}$ of real system channels, primarily due to the absence of information in the 3D map. The relationship between real and virtual NLoS components is modeled as

$$\tilde{h}_{\ell,k}^{[\text{nls}, [v_x, n_x]}} = \sqrt{\xi} \tilde{h}_{\ell,k}^{[\text{ls}, [v_x, n_x]}} + \sqrt{1 - \xi} \delta_{\ell,k} \quad \text{and} \quad \tilde{g}_k^{[\text{nls}, [v_x, n_x]}} = \sqrt{\xi} \tilde{g}_k^{[\text{ls}, [v_x, n_x]}} + \sqrt{1 - \xi} \delta_{0,k}, \quad (8)$$

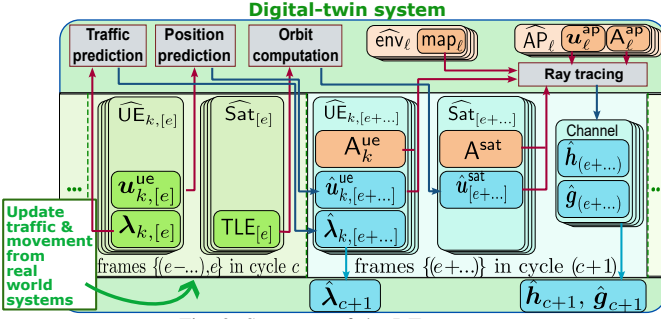


Fig. 3: Summary of the DT-system.

where $\delta_{\ell,k}$ and $\delta_{0,k}$ indicate errors caused by the absence of map information, which are assumed as complex normal random variables. $\xi \in (0, 1)$ is the correlation factor.

III. DT-BASED OPTIMIZATION PROBLEM FORMULATION

A. User Association

Let $\alpha = [\alpha_{\ell,k}^{[v_x,n_x]}]$ be the binary association variable for $x \in \{D, M\}$ where $\alpha_{\ell,k}^{[v_x,n_x]} = 1$ if AP_{ℓ} served UE_k over $RB_{[v_x,n_x]}$ for DL and $\alpha_{\ell,k}^{[v_x,n_x]} = 0$ otherwise. Note that the association with UE^x over SC v_x in BWP x is allowed only if this SC is activated, which is ensured as

$$(C4) : \alpha_{\ell,k}^{[v_x,n_x]} \leq b_{v_x,c}^x, \forall (c, \ell, k, [v_x, n_x]), x \in \{D, M\}.$$

In addition, one assumes that each RB of each AP can be assigned to at most one UE, which yields

$$(C5) : \sum_{v_k} \alpha_{\ell,k}^{[v_x,n_x]} \leq 1, \forall (c, \ell, [v_x, n_x]), x \in \{D, M\}.$$

While each UE^D can be served by multiple APs at each TS via different RBs, which is ensured as

$$(C6) : \sum_{v_{\ell}} \alpha_{\ell,k}^{[v_D,n_D]} \leq 1, \forall (c, k, [v_D, n_D]).$$

For LSat-UE association, we introduce a variable $\beta = [\beta_k^{[v_x,n_x]}]$ for $x \in \{M, S\}$ where $\beta_k^{[v_x,n_x]} = 1$ if UE_k is served by LSat over $RB_{[v_x,n_x]}$, $\beta_k^{[v_x,n_x]} = 0$ otherwise. Similar to the AP-UE association, we have

$$(C7) : \beta_k^{[v_x,n_x]} \leq b_{v_x,c}^x, \forall (c, k, [v_x, n_x]),$$

$$(C8) : \sum_{v_k} \beta_k^{[v_x,n_x]} \leq 1, \forall (c, [v_x, n_x]), x \in \{M, S\},$$

Additionally, we assume that UEs using M services can be served by both TAPs and LSat at the same time via different RBs in BWP M, which yields the constraint

$$(C9) : \sum_{v_{\ell}} \alpha_{\ell,k}^{[v_M,n_M]} + \beta_k^{[v_M,n_M]} \leq 1, \forall (c, k, [v_M, n_M]).$$

B. Service-D Transmission

Assuming that UE_k^D is served by AP_{ℓ} over $RB_{[v_D,n_D]}$, the received signal $y_k^{[v_D,n_D]}$ and its components are expressed as

$$y_k^{[v_D,n_D]} = \tilde{y}_k^{TN,[v_D,n_D]} + \zeta_k^{[v_D,n_D]}, \quad (9)$$

where $\tilde{y}_k^{TN,[v_x,n_x]} = \sum_{(i,j)} \sqrt{\alpha_{\ell,i}^{[v_x,n_x]} p_{i,j}^{[v_x,n_x]}} \tilde{h}_{i,k}^{[v_x,n_x]} x_{i,j}^{[v_x,n_x]}$; $p_{\ell,k}^{[v_x,n_x]}$ and $x_{i,k}^{[v_x,n_x]}$ are the transmit power and transmission symbol from AP_{ℓ} to UE_k over $RB_{[v_x,n_x]}$. $\zeta_k^{[v_x,n_x]} \sim \mathcal{CN}(0, \sigma_{x,k}^2)$ is the AGWN at UE_k . Hence, the SINR of UE_k is expressed as

$$\gamma_{\ell,k}^{D,[v_D,n_D]}(\mathbf{p}_c, \alpha_c) = \frac{\alpha_{\ell,k}^{[v_D,n_D]} p_{\ell,k}^{[v_D,n_D]} h_{\ell,k}^{[v_D,n_D]}}{\Psi_{\ell,k}^{[v_D,n_D]}(\mathbf{p}_c, \alpha_c) + \sigma_{D,k}^2}, \quad (10)$$

where $\Psi_{\ell,k}^{[v_x,n_x]}(\mathbf{p}_c, \alpha_c)$ is the inter-cell-interference (ICI) power,

$$\Psi_{\ell,k}^{[v_x,n_x]}(\mathbf{p}_c, \alpha_c) = \sum_{v_i \neq \ell, v_j} \alpha_{i,j}^{[v_x,n_x]} p_{i,j}^{[v_x,n_x]} h_{i,k}^{[v_x,n_x]}, \quad (11)$$

with $(\mathbf{p}_c, \alpha_c) \triangleq \{(p_{\ell,k}^{[v_x,n_x]}, \alpha_{\ell,k}^{[v_x,n_x]}) | \forall (\ell, k, [v_x, n_x]), x \in \{D, M\}\}$ and $h_{\ell,k}^{[v_x,n_x]} = |\tilde{h}_{\ell,k}^{[v_x,n_x]}|^2$. Due to the delay-sensitive requirement, the short packet framework is used to model the transmission of D service. Hence, the aggregated achievable rate of UE_k^D served by AP_{ℓ} at SF s can be expressed as [29]

$$R_{\ell,k,[s]}^{SF,D}(\mathbf{p}_c, \alpha_c) = w_D \left[\sum_{v_{(v_D,n_D)}} \log_2 (1 + \gamma_{\ell,k}^{D,[v_D,n_D]}(\mathbf{p}_c, \alpha_c)) \right] \quad (12)$$

$$-1/\ln(2) \alpha_{\ell,k}^{[v_D,n_D]} \sqrt{V_{\ell,k}^{[v_D,n_D]}} Q^{-1}(P_{\epsilon}) / \sqrt{\sum_{v_{(v_D,n_D)}} \alpha_{\ell,k}^{[v_D,n_D]} T_{\ell,k} w_D},$$

where $V_{\ell,k}^{[v_D,n_D]} = 1 - (1 + \gamma_{\ell,k}^{D,[v_D,n_D]}(\mathbf{p}_c, \alpha_c))^{-2}$, $Q^{-1}(\cdot)$ and P_{ϵ} are the channel dispersion, the inverse of the Q-function, and the error probability. One can see that the channel dispersion can be approximated as $V_{\ell,k}^{[v_D,n_D]} \approx 1$ for a sufficiently high $\gamma_{\ell,k}^{D,[v_D,n_D]}(\mathbf{p}_c, \alpha_c) \geq \gamma_0^D$ with $\gamma_0^D \geq 5$ dB [30]. Regarding this approximation, we consider the following constraint

$$(C10) : \gamma_{\ell,k}^{D,[v_D,n_D]}(\mathbf{p}_c, \alpha_c) \geq \alpha_{\ell,k}^{[v_D,n_D]} \gamma_0^D, \forall (\ell, k, v_D, n_D).$$

Subsequently, $R_{\ell,k,[s]}^{SF,D}(\mathbf{p}_c, \alpha_c)$ can be rewritten as

$$R_{\ell,k,[s]}^{SF,D}(\mathbf{p}_c, \alpha_c) = w_D \sum_{v_{(v_D,n_D)}} \log_2 (1 + \gamma_{\ell,k}^{D,[v_D,n_D]}(\mathbf{p}_c, \alpha_c)) - \chi_D \sqrt{\sum_{v_{(v_D,n_D)}} \alpha_{\ell,k}^{[v_D,n_D]}}, \quad (13)$$

where $\chi_D = \sqrt{V_{\ell,k}^{[v_D,n_D]} Q^{-1}(P_{\epsilon}) / \ln(2)}$ and $V \approx V_{\ell,k}^{[v_D,n_D]} \approx 1$.

C. Service-M Transmission

In this BWP, UEs can be served by APs and the LSat. The received signal $y_k^{M,[v_M,n_M]}$ at UE_k^M over $RB_{[v_M,n_M]}$ and its components is expressed as

$$y_k^{M,[v_M,n_M]} = \tilde{y}_k^{TN,[v_M,n_M]} + \tilde{y}_k^{Sat,M,[v_M,n_M]} + \zeta_k^{[v_M,n_M]}, \quad (14)$$

$$\tilde{y}_k^{Sat,M,[v_M,n_M]} \triangleq \sum_{v_j} \sqrt{p_{j,[v_M,n_M]}^{[v_M,n_M]} p_{0,j}^{[v_M,n_M]}} \tilde{g}_k^{[v_M,n_M]} x_j^{[v_M,n_M]}, \quad (15)$$

where $p_{0,k}^{[v_x,n_x]}$ is the transmit power from the LSat to UE_k over $RB_{[v_x,n_x]}$, and $\tilde{g}_k^{[v_x,n_x]} = |\tilde{g}_k^{[v_x,n_x]}|^2$. For brevity, let's define $(\mathbf{p}_{0,c}, \beta_c) \triangleq \{(p_{0,k}^{[v_x,n_x]}, \beta_k^{[v_x,n_x]}) | \forall (k, v_x, n_x), x \in \{M, S\}\}$ and $\mathbf{P}_c \triangleq \{\mathbf{p}_c, \mathbf{p}_{0,c}\}$. Hereafter, argument \mathbf{p}_c in defined functions is replaced appropriately by \mathbf{P}_c .

1) *TN-served UEs*: Assuming that UE_k^M is served by AP_{ℓ} , the corresponding SINR is expressed as

$$\gamma_{\ell,k}^{M,[v_M,n_M]}(\mathbf{p}_c, \alpha_c, \beta_c) = \frac{\alpha_{\ell,k}^{[v_M,n_M]} p_{\ell,k}^{[v_M,n_M]} h_{\ell,k}^{[v_M,n_M]}}{\Psi_{\ell,k}^{[v_M,n_M]}(\mathbf{p}_c, \alpha_c) + \Theta_k^{TN,[v_M,n_M]}(\mathbf{p}_c, \beta_c) + \sigma_{M,k}^2}, \quad (16)$$

where $\Psi_{\ell,k}^{[v_M,n_M]}$ is defined in (11) and $\Theta_k^{TN,[v_M,n_M]}(\mathbf{p}_c, \beta_c)$ is the inter-system-interference (ISyI) caused by the LSat to UE_k^M served by TN over $RB_{[v_M,n_M]}$ which is given as

$$\Theta_k^{TN,[v_M,n_M]}(\mathbf{p}_c, \beta_c) = \sum_{v_j} \beta_j^{[v_M,n_M]} p_{0,j}^{[v_M,n_M]} g_k^{[v_M,n_M]}, \quad (17)$$

The corresponding achievable rate over $RB_{[v_M,n_M]}$ and the aggregated rate at RB time n_M are expressed as

$$R_{\ell,k}^{M,[v_M,n_M]}(\mathbf{p}_c, \alpha_c, \beta_c) = w_M \log_2 (1 + \gamma_{\ell,k}^{M,[v_M,n_M]}(\mathbf{p}_c, \alpha_c, \beta_c)), \quad (18a)$$

$$R_{\ell,k}^{M,[n_M]}(\mathbf{p}_c, \alpha_c, \beta_c) = \sum_{v_{v_M} \in \mathcal{V}_M} R_{\ell,k}^{M,[v_M,n_M]}(\mathbf{p}_c, \alpha_c, \beta_c). \quad (18b)$$

2) *UE served by SatNet*: Assuming that UE_k^M is served by the LSat over $RB_{[v_M,n_M]}$, the corresponding SINR is given as

$$\gamma_{0,k}^{M,[v_M,n_M]}(\mathbf{p}_c, \alpha_c, \beta_c) = \frac{\beta_k^{[v_M,n_M]} p_{0,k}^{[v_M,n_M]} g_k^{[v_M,n_M]}}{\Theta_k^{Sat,[v_M,n_M]}(\mathbf{p}_c, \alpha_c) + \sigma_{M,k}^2}, \quad (19)$$

where $\Theta_k^{Sat,[v_M,n_M]}(\mathbf{p}_c, \alpha_c)$ is the ISyI caused by TAPs to UE_k^M served by the LSat which is defined as

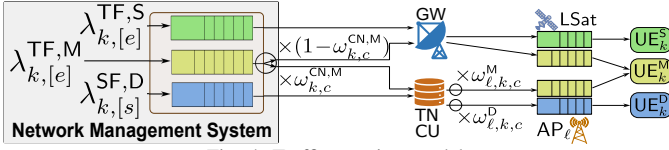


Fig. 4: Traffic steering model.

$$\Theta_k^{\text{Sat},[\nu_M, n_M]}(\mathbf{P}_c, \alpha_c) = \sum_{\forall(i,j)} \alpha_{i,j}^{[\nu_M, n_M]} p_{i,j}^{[\nu_M, n_M]} h_{i,k}^{[\nu_M, n_M]}. \quad (20)$$

Therefore, the achievable rate over $\text{RB}_{[\nu_M, n_M]}$ and the aggregated rate at RB time n_M of UE_k^M served by the LSat can be respectively expressed as

$$R_{0,k}^{M, [\nu_M, n_M]}(\mathbf{P}_c, \alpha_c, \beta_c) = w_M \log_2 \left(1 + \gamma_{0,k}^{M, [\nu_M, n_M]}(\mathbf{P}_c, \alpha_c, \beta_c) \right), \quad (21a)$$

$$R_{0,k}^{M, [n_M]}(\mathbf{P}_c, \alpha_c, \beta_c) = \sum_{\forall \nu_M \in \mathcal{V}_M} R_{0,k}^{M, [\nu_M, n_M]}(\mathbf{P}_c, \alpha_c, \beta_c). \quad (21b)$$

D. Service-S Transmission

In this BWP, if UE_k^S is served by LSat over $\text{RB}_{[\nu_S, n_S]}$, the corresponding SNR is given by

$$\gamma_{0,k}^{S, [\nu_S, n_S]}(\mathbf{P}_c, \beta_c) = (\beta_k^{[\nu_S, n_S]} p_{0,k}^{[\nu_S, n_S]} g_{0,k}^{[\nu_S, n_S]}) / \sigma_{S,k}^2, \quad (22)$$

Therefore, the achievable rate over $\text{RB}_{[\nu_S, n_S]}$ and the aggregated rate at RB time n_S of UE_k^S can be expressed as

$$R_{0,k}^{S, [\nu_S, n_S]}(\mathbf{P}_c, \beta_c) = w_S \log_2 \left(1 + \gamma_{0,k}^{S, [\nu_S, n_S]}(\mathbf{P}_c, \beta_c) \right), \quad (23a)$$

$$R_{0,k}^{S, [n_S]}(\mathbf{P}_c, \beta_c) = \sum_{\forall \nu_S \in \mathcal{V}_S} R_{0,k}^{S, [\nu_S, n_S]}(\mathbf{P}_c, \beta_c). \quad (23b)$$

Regarding the TAP/LSat power budget, one must satisfy

$$(C11) : \sum_{x \in \{D, M\}} \sum_{\forall k} \sum_{\forall \nu_x \in \mathcal{V}_x} p_{\ell, k}^{[\nu_x, n_x]} \leq p_{\text{AP}, \ell}^{\max}, \forall (\ell, t),$$

$$(C12) : \sum_{x \in \{M, S\}} \sum_{\forall k} \sum_{\forall \nu_x \in \mathcal{V}_x} p_{0, k}^{[\nu_x, n_x]} \leq p_{\text{LSat}}^{\max}, \forall t.$$

E. Traffic and Queuing Model

Regarding latency tolerance, different time scales are applied to serve UEs associated with different services. Specifically, the arrival data of **M** and **S** services are buffered and scheduled for transmission in the following frame, whereas the data stream of **D** services is processed at the SF time scale to meet stringent latency requirements. Assuming K traffic flows arriving the CN due to K UEs. Denote $\lambda_{[e]}^{\text{TF}, M} = \{\lambda_{k, [e]}^{\text{TF}, M} | \forall k \in \mathcal{K}_M\}$, $\lambda_{[e]}^{\text{TF}, S} = \{\lambda_{k, [e]}^{\text{TF}, S} | \forall k \in \mathcal{K}_S\}$, and $\lambda_{[s]}^{\text{SF}, D} = \{\lambda_{k, [s]}^{\text{SF}, D} | \forall k \in \mathcal{K}_D\}$, where $\lambda_{k, [e]}^{\text{TF}, M}$, $\lambda_{k, [e]}^{\text{TF}, S}$, and $\lambda_{k, [s]}^{\text{SF}, D}$ are the data arrival rates of UE_k^M , UE_k^S at frame e , and of UE_j^D at SF s , respectively. Additionally, the traffic rates in cycle c and frame e are denoted by λ_c and λ_e .

1) *Traffic Steering*: As depicted in Fig. 4, at the CN, the **D** and **S** traffic flows are routed to the TNs and SatNet, respectively, while **M** traffic is split and dynamically steered to both domains. Subsequently, at the TCU, the **D** and **M** flows are further directed to TAPs due to a TN steering scheduler.

For **M**-traffic steering, we introduce variables $\omega_c^{\text{CN}, M} = [\omega_{k, c}^{\text{CN}, M}], \forall k \in \mathcal{K}_M$, where $\omega_{k, c}^{\text{CN}, M} \in [0, 1]$ and $(1 - \omega_{k, c}^{\text{CN}, M})$ are the portions of UE_k^M 's traffic which are steered to TN and SatNet in cycle c , respectively. In the TN, let $\omega_c^x = [\omega_{\ell, k, c}^x], \forall (\ell, k) \in (\mathcal{L} \times \mathcal{K}_x), x \in \{D, M\}$ be the TN steering variables, wherein $\omega_{\ell, k, c}^x \in [0, 1]$ indicates the flow-split portion of service $x \in \{D, M\}$ from TCU to AP_ℓ in cycle c . Besides, the integrity of traffic flows is ensured by

$$(C13) : \sum_{\forall \ell \in \mathcal{L}} \omega_{\ell, k, c}^x = 1, \forall (c, k), x \in \{D, M\}.$$

Subsequently, the data arrival of **D** service in SF s , and that of **M** and **S** services in frame e at AP_ℓ /LSat corresponding to UEs are respectively expressed as

$$\lambda_{\ell, k, [s]}^{\text{SF}, D} = \omega_{\ell, k, c}^D \lambda_{k, [s]}^{\text{SF}, D}, \forall (\ell, k, s) \in \mathcal{L} \times \mathcal{K}_D \times \mathcal{T}_{\text{SF}}^{\text{Cy}, c}, \forall c \quad (24a)$$

$$\lambda_{\ell, k, [e]}^{\text{TF}, M} = \omega_{k, c}^{\text{CN}, M} \omega_{\ell, k, c}^M \lambda_{k, [e]}^{\text{TF}, M}, \forall (\ell, k, e) \in \mathcal{L} \times \mathcal{K}_M \times \mathcal{T}_{\text{TF}}^{\text{Cy}, c}, \forall c, \quad (24b)$$

$$\lambda_{0, k, [e]}^{\text{TF}, M} = (1 - \omega_{k, c}^{\text{CN}, M}) \lambda_{k, [e]}^{\text{TF}, M}, \forall (k, e) \in \mathcal{K}_M \times \mathcal{T}_{\text{TF}}^{\text{Cy}, c}, \forall c, \quad (24c)$$

$$\lambda_{0, k, [e]}^{\text{TF}, S} = \lambda_{k, [e]}^{\text{TF}, S}, \forall k \in \mathcal{K}_S, \forall e, \quad (24d)$$

where $\mathcal{T}_{\text{TF}}^{\text{Cy}, c}$ and $\mathcal{T}_{\text{SF}}^{\text{Cy}, c}$ are the frame and SF sets in cycle c . For **D** service, the SF time-scale data-processing requirement is cast by the following constraint,

$$(C14) : T_{\text{D}} R_{\ell, k, [s]}^{\text{SF}, D} \geq \lambda_{\ell, k, [s]}^{\text{SF}, D}, \forall \ell, \forall k \in \mathcal{K}_D, \forall s.$$

2) *Service queues*: Assume that TAPs and LSat are equipped with service-specific buffers. Each TAP/LSat is assumed to maintain separate queues for the UE data flows [25]. Subsequently, let $q_{\ell, k}^{M, [n_M]}, q_{0, k}^{M, [n_M]},$ and $q_{0, k}^{S, [n_S]}$ be the queue lengths (QLs) at AP_ℓ /LSat of flow k of services **M**, **S** at each RB time, the QL evolution over time is expressed as

$$q_{\ell, k}^{M, [n_M+1]} = \left[q_{\ell, k}^{M, [n_M]} + \lambda_{\ell, k}^{M, [n_M]} - T_{\text{M}} R_{\ell, k}^{M, [n_M]} \right]^+, \forall \ell, \forall k \in \mathcal{K}_M, \quad (25a)$$

$$q_{0, k}^{x, [n_x+1]} = \left[q_{0, k}^{x, [n_x]} + \lambda_{0, k}^{x, [n_x]} - T_x R_{0, k}^{x, [n_x]} \right]^+, \forall k \in \mathcal{K}_x, \forall x \in \{M, S\}, \quad (25b)$$

where $[\cdot]^+ = \max\{0, \cdot\}$; $\lambda_{\ell, k}^{M, [n_M]}, \lambda_{0, k}^{M, [n_M]},$ and $\lambda_{0, k}^{S, [n_S]}$ are intermediate data arrival notations with setting

$$\begin{cases} \lambda_{\ell, k}^{M, [n_M]} = \lambda_{\ell, k, [e]}^{\text{TF}, M}, \lambda_{0, k}^{x, [n_x]} = \lambda_{0, k, [e]}^{\text{TF}, x} & \text{if } \text{mod}(n_x, 10N_x) = 1, \\ \lambda_{\ell, k}^{M, [n_M]} = 0, \lambda_{0, k}^{x, [n_x]} = 0 & \text{otherwise,} \end{cases} \quad (26)$$

where $\{n_x | \text{mod}(n_x, 10N_x) = 1\}$ indicates first RB time of each frame. To maintain stability, the total QL of each service $x \in \{M, S\}$ at AP_ℓ /LSat must satisfy [25]

$$(C15) : q_{\ell}^{M, [n_M]} = \sum_{\forall k \in \mathcal{K}_M} q_{\ell, k}^{M, [n_M]} \leq q_{\ell}^{M, \max}, \forall (\ell, n_M),$$

$$(C16) : q_0^{x, [n_x]} = \sum_{\forall k \in \mathcal{K}_x} q_{0, k}^{x, [n_x]} \leq q_0^{x, \max}, \forall n_x, x \in \{M, S\},$$

where $q_{\ell}^{M, \max}$ and $q_0^{x, \max}$ are the maximum QL of AP_ℓ and LSat for corresponding services, respectively. For convenience, let's denote $\mathbf{q}_c^{\text{TN}} = \{q_{\ell, k}^{M, [n_M]} | \forall \ell, \forall k, \forall n_M \in \mathcal{T}_{\text{M}}^{\text{Cy}, c}\}$, $\mathbf{q}_c^{\text{Sat}} = \{q_{0, k}^{x, [n_x]} | \forall k, \forall n_x \in \mathcal{T}_x^{\text{Cy}, c}, \forall x \in \{M, S\}\}$, and $\mathbf{q}_c = \{\mathbf{q}_c^{\text{TN}}, \mathbf{q}_c^{\text{Sat}}\}$.

Remark 2. The arrival data packet of **D** services is completely served within the next SF, as ensured by constraint (C14). Hence, the buffer of **D** services is cleared after each SF, and the QL of **D** services is not considered.

F. Problem Formulation

Typically, the uneven traffic demand of services and the inefficient spectrum utilization may lead to congestion in systems. Hence, this work aims to minimize the system congestion, i.e., the mean system QL, by optimizing the BWA, traffic split decision, AP-UE and LSat-UE associations, RB assignment, and power control. As a result, the utility function is the total average QL per RB time of **M** and **S** services at TAPs and LSats in each cycle c defined as

$$f_{\text{obj}}(\mathbf{q}_c) = \frac{1}{N_M N_{\text{SF}}} \sum_{\forall n_M \in \mathcal{T}_{\text{M}}^{\text{Cy}, c}, \forall \ell} q_{\ell}^{M, [n_M]} + \sum_{x \in \{M, S\}} \frac{1}{N_x N_{\text{SF}}} \sum_{\forall n_x \in \mathcal{T}_x^{\text{Cy}, c}} q_0^{x, [n_x]}. \quad (27)$$

Subsequently, two problems, “DT-JointRA” and “RT-Refine”, will be studied. The former optimizes systems for each cycle c and the latter optimizes TN short-term decisions for each SF, which are solved at the CNC and TCU, respectively.

1) *DT-JointRA Problem*: For cycle c , we consider
 $(\mathcal{P}_0)_c : \min_{\mathbf{b}_c, \omega_c, \mathbf{P}_c, \alpha_c, \beta_c, \mathbf{q}_c} f_{\text{obj}}(\mathbf{q}_c)$ s.t. constraints (C1)–(C16),
(C0) : $b_{v_x, c}^x, \alpha_{\ell, k}^{[v_x, n_x]}, \beta_k^{[v_x, n_x]} \in \{0, 1\}, \forall (\ell, k, v_x, n_x, c)$.

2) *RT-Refine Problem*: Regarding implementation aspects, problem $(\mathcal{P}_0)_c$ requires future information $\{\mathbf{h}_c, \mathbf{g}_c, \lambda_c\}$ in cycle c which is challenging in practice. Assuming that the predicted information $\{\hat{\mathbf{h}}_c, \hat{\mathbf{g}}_c, \hat{\lambda}_c\}$ is used instead of $\{\mathbf{h}_c, \mathbf{g}_c, \lambda_c\}$, the corresponding solution should be adjusted appropriately with actual information. Hence, this section formulates the refinement problem to adjust the obtained solution at each SF by re-optimizing TN short-term decisions. However, due to the long propagation distance in SatNet, the channel estimation and RA in SatNet at each SF are challenging. Hence, the given RA in SatNet can remain unchanged.

Let's call UEs served by TAPs and LSat as TN UEs and SatNet UEs. Assuming that TAPs only estimate TN UE CSIs, the predicted CSIs of SatNet UEs should be used. For a given SatCom RA, the channel uncertainty of M UEs served by LSat leads to errors in the ISyI power $\Theta_k^{\text{TN}, [v_M, n_M]}$ and $\Theta_k^{\text{Sat}, [v_M, n_M]}$. Hence, we impose the interference margin coefficient $\kappa \geq 1$ and use $\hat{\Theta}_k^{\text{TN}, [v_M, n_M]} = \kappa \Theta_k^{\text{TN}, [v_M, n_M]}$ and $\hat{\Theta}_k^{\text{Sat}, [v_M, n_M]} = \kappa \Theta_k^{\text{Sat}, [v_M, n_M]}$ for refinement problem.

Let \mathbf{h}_e^* be the channel gain matrix in frame e where CSIs of TN UEs are actual while those of SatNet UEs are extracted from $\hat{\mathbf{h}}_e$. Based on channel gains $\{\mathbf{h}_e^*, \hat{\mathbf{g}}_e\}$ and actual traffic λ_e in frame e , for a fixed $\{\mathbf{b}_c, \omega_c, \mathbf{p}_0, \beta_c\}$, the refinement problem for TN short-term decisions at SF s is formulated as

$$(\mathcal{P}_0^{\text{refi}})_s : \min_{\mathbf{p}[s], \alpha[s], \mathbf{q}[s]} f_{\text{obj}}(\mathbf{q}[s])$$

s.t. (C4)_s–(C6)_s, (C9)_s, (C10)_s, (C11)_s, (C14)_s, (C15)'_s, (C16)'_s

where index s used in $\mathbf{x}[s]$ and $(Cx)_s$ indicates time index adaptation to SF s for variable \mathbf{x} and constraint (Cx) , $(C15)'$ and $(C16)'$ are the constraint revised from $(C15)$ and $(C16)$ in which terms $\hat{\Theta}_k^{\text{TN}, [v_M, n_M]}$ and $\hat{\Theta}_k^{\text{Sat}, [v_M, n_M]}$ are used instead of $\Theta_k^{\text{TN}, [v_M, n_M]}$ and $\Theta_k^{\text{Sat}, [v_M, n_M]}$ in rate functions, respectively.

Challenges in solving $(\mathcal{P}_0)_c$ and $(\mathcal{P}_0^{\text{refi}})_s$: these problems contain the non-convex constraints, SINR and rate functions. Especially, problem $(\mathcal{P}_0)_c$ further consists of both continuous and binary variables. Hence, $(\mathcal{P}_0^{\text{refi}})_s$ and $(\mathcal{P}_0)_c$ are non-convex and MINLP problems. Additionally, the unknown channel and traffic information in $(\mathcal{P}_0)_c$ makes it more complicated.

3) *Overall workflow*: Let $\{\hat{\mathbf{x}}_c\}$ and $\{\mathbf{x}_c\}$ with $\mathbf{x} \in \{\mathbf{h}, \mathbf{g}, \lambda, \mathbf{u}^{\text{ue}}, \mathbf{u}^{\text{sat}}, \text{TLE}\}$ be the DT-virtual and real information vector in cycle c , the overall workflow is summarized as

- ① Based on the updated UE position $\hat{\mathbf{u}}_{c-1}^{\text{ue}}$, orbit information TLE_{c-1} , and traffic λ_{c-1} in cycle $(c-1)$, the DT model first predicts $\hat{\lambda}_c$, $\{\hat{\mathbf{u}}_c^{\text{ue}}, \hat{\mathbf{u}}_c^{\text{sat}}\}$, and then $\{\hat{\mathbf{h}}_c, \hat{\mathbf{g}}_c\}$ in cycle c .
- ② Based on $\{\hat{\mathbf{h}}_c, \hat{\mathbf{g}}_c, \hat{\lambda}_c\}$, problem $(\mathcal{P}_0)_c$ is solved at the CNC to obtain long-term decisions and preliminary estimates of short-term ones $\{\mathbf{b}_c, \omega_c, \mathbf{P}_c, \alpha_c, \beta_c\}$ for cycle c .
- ③ For each frame e in cycle c , using channel gain \mathbf{h}_e^* , arrival data rate λ_e in the real system, and given decisions $\{\mathbf{b}_c, \omega_c, \mathbf{p}_0, \beta_c\}$, the initial power control, UE association, and RB assignment $\{\mathbf{p}_c, \alpha_c\}$ in the TN, which are outcomes of step 2, are refined by solving problem $(\mathcal{P}_0^{\text{refi}})_s$ at TCU at each SF s in frame e .

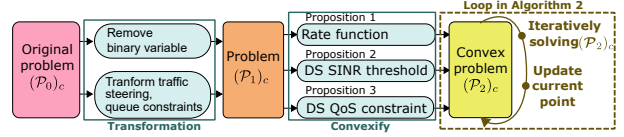


Fig. 5: Developing workflow.

Algorithm 1 DT-BASED PREDICTION

- 1: **Input**: Actual information $\{\lambda_{c-1}, \mathbf{u}^{\text{ue}}_{c-1}, \text{TLE}_{c-1}\}$ in cycle $(c-1)$.
- 2: Predict $\{\hat{\mathbf{u}}_c^{\text{ue}}, \hat{\mathbf{u}}_c^{\text{sat}}\}$ and construct $\{\hat{\mathbf{u}}_e^{\text{ue}} | \forall e \in \mathcal{T}_{\text{TF}}^{\text{Cy}, c}\}$.
- 3: Predict $\{\hat{\lambda}_c, \hat{\lambda}_e\}$ by (7), (28).
- 4: Construct $\{\hat{\mathbf{h}}_c, \hat{\mathbf{g}}_c\}$ by using $\hat{\mathbf{u}}_e^{\text{ue}}$ with $\xi = 1$.
- 5: **Output**: Predicted information $\{\hat{\mathbf{h}}_c, \hat{\mathbf{g}}_c, \hat{\lambda}_c\}$.

IV. PROPOSED SOLUTIONS

This section first proposes the solution for problem $(\mathcal{P}_0)_c$. Subsequently, the solution for the problem $(\mathcal{P}_0^{\text{refi}})_s$ is proposed to refine TN short-term decisions with actual information. The solution workflows are summarized in Figs. 5 and 6.

A. DT-based Prediction

At the beginning of every cycle, DT model needs the updated UEs position and LSat orbit information for channel prediction. Assuming that the cycle duration is sufficiently small, the changes in the movement trend of UEs and velocity are negligible. Hence, with a given updated route and velocity in cycle $(c-1)$, the UE position in cycle c can be estimated by the approach given in [16]. Subsequently, channel components in cycle c are identified by (7). Based on output $\text{chan}_c \triangleq \{\text{chan}_e | \forall e \in \mathcal{T}_{\text{TF}}^{\text{Cy}, c}\}$, channel gain $\{\hat{\mathbf{h}}_c, \hat{\mathbf{g}}_c\}$ used for problem $(\mathcal{P}_0)_c$ is computed with DT channel coefficient $\xi = 1$.

Regarding UE traffic, one can assume that UEs continue to use specific services over a given time duration. As a result, their traffic pattern and arrival traffic remain relatively stable. Therefore, the arrival data in cycle c can be estimated by the average in cycle $(c-1)$ as

$$\hat{\lambda}_{k, [s]}^{\text{SF}, \text{D}} = \frac{1}{N_{\text{SF}}} \sum_{s' \in \mathcal{T}_{\text{SF}}^{\text{Cy}, c-1}} \lambda_{k, [s']}^{\text{SF}, \text{D}}, \quad \forall s \in \mathcal{T}_{\text{SF}}^{\text{Cy}, c}, \quad (28a)$$

$$\hat{\lambda}_{k, [e]}^{\text{TF}, x} = \frac{1}{N_{\text{TF}}} \sum_{e' \in \mathcal{T}_{\text{TF}}^{\text{Cy}, c-1}} \lambda_{k, [e']}^{\text{TF}, x}, \quad \forall e \in \mathcal{T}_{\text{TF}}^{\text{Cy}, c}, x \in \{\text{M}, \text{S}\}. \quad (28b)$$

The DT-based prediction mechanism is summarized in Alg. 1.

B. DT-JointRA Solution

1) *Compressed-Sensing-Based Relaxation*: Considering the system model and the optimization problem $(\mathcal{P}_0)_c$, one can see the relationship between the binary variable $\{\alpha_c, \beta_c\}$ and the continuous variable \mathbf{P}_c as follows. Consider $\text{RB}_{[v_x, n_x]}$:

- If AP _{ℓ} serves UE _{k} $\Rightarrow \alpha_{\ell, k}^{[v_x, n_x]} = 1, p_{\ell, k}^{[v_x, n_x]} > 0$;
if AP _{ℓ} does not serve UE _{k} $\alpha_{\ell, k}^{[v_x, n_x]} = 0, p_{\ell, k}^{[v_x, n_x]} = 0$;
- If the LSat serves UE _{k} $\Rightarrow \beta_k^{[v_x, n_x]} = 1, p_{0, k}^{[v_x, n_x]} > 0$;
if the LSat does not serve UE _{k} $\beta_k^{[v_x, n_x]} = 0, p_{0, k}^{[v_x, n_x]} = 0$.

Based on this relationship, the binary variables α_c and β_c can be respectively represented by the continuous one \mathbf{P}_c as

$$\alpha_{\ell, k}^{[v_x, n_x]} = \|p_{\ell, k}^{[v_x, n_x]}\|_0, \quad \beta_k^{[v_x, n_x]} = \|p_{0, k}^{[v_x, n_x]}\|_0. \quad (29)$$

Besides, consider (C4), (C7), one can see that SC v_x is activated in cycle c , i.e., $b_{v_x, c}^x = 1$, only if it is used by at least one TAP/LSat-UE link at any RB time $n_x \in \mathcal{T}_x^{\text{Cy}, c}$, i.e., $\alpha_{\ell, k}^{[v_x, n_x]} = 1$ or $\beta_k^{[v_x, n_x]} = 1$. Combining (29), \mathbf{b}_c is rewritten as

$$b_{v_D,c}^D = \left\| \sum_{\forall(\ell,k), \forall n_D \in \mathcal{T}_D^{Cyc,c}} \alpha_{\ell,k}^{[v_D,n_D]} \right\|_0 = \|p_{v_D,c}^D\|_0, \quad \forall(v_D, c), \quad (30a)$$

$$b_{v_M,c}^M = \left\| \sum_{\forall(\ell,k), \forall n_M \in \mathcal{T}_M^{Cyc,c}} \alpha_{\ell,k}^{[v_M,n_M]} + \sum_{\forall k, \forall n_M \in \mathcal{T}_M^{Cyc,c}} \beta_k^{[v_M,n_M]} \right\|_0 = \|P_{v_M,c}^M\|_0, \quad \forall(v_M, c), \quad (30b)$$

$$b_{v_S,c}^S = \left\| \sum_{\forall k, \forall n_S \in \mathcal{T}_S^{Cyc,c}} \beta_k^{[v_S,n_S]} \right\|_0 = \|p_{0,v_S,c}^S\|_0, \quad \forall(v_S, c). \quad (30c)$$

where $P_{v_M,c}^M = p_{v_M,c}^M + p_{0,v_M,c}^M$, $p_{v_X,c}^X = \sum_{\forall(\ell,k), \forall n_X \in \mathcal{T}_X^{Cyc,c}} p_{\ell,k}^{[v_X,n_X]}$ and $P_{v_X,c}^X = \sum_{\forall k, \forall n_X \in \mathcal{T}_X^{Cyc,c}} p_{0,k}^{[v_X,n_X]}$. Thanks to relationship (30), constraints (C4), (C7) can be omitted.

Exploiting (29), the binary components can be replaced by the corresponding ℓ_0 -norm components. Moreover, the binary variables in the production components and the binary arguments of SINR/rate functions can be omitted. Specifically, $R_{\ell,k,[s]}^{SF,D}(\mathbf{P}_c, \alpha_c)$ is reformulated as

$$R_{\ell,k,[s]}^{SF,D}(\mathbf{P}_c) = w_D \sum_{\forall(v_D, n_D)} \log_2 (1 + \gamma_{\ell,k}^{D,[v_D,n_D]}(\mathbf{P}_c)) - \chi_D \sqrt{\sum_{\forall(v_D, n_D)} \|p_{\ell,k}^{[v_D,n_D]}\|_0}, \quad (31)$$

Subsequently, the ℓ_0 -norm component $\|x\|_0, \forall x \geq 0$, can be approximated by concave function $\mathcal{F}_{\text{apx}}(x) \triangleq 1 - e^{-x/\epsilon}, 0 < \epsilon \ll 1$, as $\|x\|_0 \approx \mathcal{F}_{\text{apx}}(x)$. Let $\mathcal{F}_{\text{apx}}^{(i)}(x)$ be an upper bound of $\mathcal{F}_{\text{apx}}(x)$ at feasible point $(x^{(i)})$, the ℓ_0 -norm components in (29) and (30) can be approximated at iteration i as

$$\|\tau\|_0 \approx \mathcal{F}_{\text{apx}}(\tau) \leq \mathcal{F}_{\text{apx}}^{(i)}(\tau), \quad \tau \in \{p_{\ell,k}^{[v_X,n_X]}, p_{0,k}^{[v_X,n_X]}, p_{v_X,c}^X, p_{0,v_X,c}^X, P_{v_X,c}^X\}, \quad (32)$$

where upper bound $\mathcal{F}_{\text{apx}}^{(i)}(x)$ can be obtained based on [16] as

$$\mathcal{F}_{\text{apx}}(x) \leq \mathcal{F}_{\text{apx}}^{(i)}(x) \triangleq 1/\epsilon \exp(-x^{(i)}/\epsilon)(x - x^{(i)} - \epsilon) + 1. \quad (33)$$

Utilize (29), (30), and (32), by replacing binary component $b_{v_X,c}^X, \alpha_{\ell,k}^{[v_X,n_X]}, \beta_k^{[v_X,n_X]}$ by the corresponding approximated terms $\mathcal{F}_{\text{apx}}^{(i)}(\cdot)$ at iteration i , constraints (C1) – (C3), (C5), (C6), (C8) – (C9) are directly transformed into convex ones so-called (C1) – (C3), (C5), (C6), (C8) – (C9); and (C10) is approximated as

$$(C10) : \gamma_{\ell,k}^{D,[v_D,n_D]}(\mathbf{P}_c) \geq \mathcal{F}_{\text{apx}}^{(i)}(p_{\ell,k}^{[v_D,n_D]}) \gamma_0^D, \quad \forall(\ell, k, v_D, n_D).$$

2) *Transform Traffic and Queue Constraints:* (C14) – (C16) are non-convex due to non-convex rate functions, coupling between traffic steering variables, and QL dependency. First, we introduce variable $\bar{\omega} = \{\bar{\omega}_{\ell,k,c}^X | \forall(\ell, k, c, x)\}$ and use it instead of $\omega_{k,c}^{\text{CN},M}$ and $\omega_{\ell,k,c}^X$ with the relationship

$$\omega_{\ell,k,c}^D = \omega_{\ell,k,c}^D \quad \text{and} \quad \bar{\omega}_{\ell,k,c}^M = \omega_{k,c}^{\text{CN},M} \omega_{\ell,k,c}^M, \quad (34)$$

Hence, constraint (C13) is rewritten for the D service as

$$(C13) : \sum_{\forall \ell \in \mathcal{L}} \bar{\omega}_{\ell,k,c}^D = 1, \quad \forall k \in \mathcal{K}_D, \forall c.$$

The traffic arrival rates (24a)–(24c) are rewritten as

$$\lambda_{\ell,k,[s]}^{SF,D} = \bar{\omega}_{\ell,k,c}^D \lambda_{k,[s]}^{SF,D}, \quad \forall \ell, \forall k \in \mathcal{K}_D, \forall s \in \mathcal{T}_D^{Cyc,c}, \forall c, \quad (35a)$$

$$\lambda_{\ell,k,[e]}^{TF,M} = \bar{\omega}_{\ell,k,c}^M \lambda_{k,[e]}^{TF,M}, \quad \forall \ell, \forall k \in \mathcal{K}_M, \forall e \in \mathcal{T}_M^{Cyc,c}, \forall c, \quad (35b)$$

$$\lambda_{0,k,[e]}^{TF,M} = (1 - \sum_{\forall \ell} \bar{\omega}_{\ell,k,c}^M) \lambda_{k,[e]}^{TF,M}, \quad \forall k \in \mathcal{K}_M, \forall e \in \mathcal{T}_M^{Cyc,c}, \forall c. \quad (35c)$$

Remark 3. The integrity of the M traffic is ensured thanks to representation (34), (35). Particularly, based on (34), (24c) is rewritten by (35c) due to $\sum_{\forall \ell} \bar{\omega}_{\ell,k,c}^M = \omega_{k,c}^{\text{CN},M}$. Since $\sum_{\forall \ell} \lambda_{\ell,k,[e]}^{TF,M} + \lambda_{0,k,[e]}^{TF,M} = \lambda_{k,[e]}$, the integrity is ensured.

Subsequently, we introduce slack variables $\bar{q}_c = \{\bar{q}_{\ell,k}^{X,[n_X]}, \bar{q}_{0,k}^{X,[n_X]} | \forall(\ell, k), \forall n_X \in \mathcal{T}_X^{Cyc,c}, \forall x \in \{M, S\}\}$ as the QL upper bound and $r_c = \{r_{\ell,k}^{X,[v_X,n_X]}, r_{0,k}^{X,[v_X,n_X]}, r_{\ell,k,[s]}^{SF,D} | \forall(\ell, k, s, v_X, n_X), \forall x \in \mathcal{S}\}$ as the rate's lower bound; and transform (25) and (C14) – (C16) as

(C14) : $T_D r_{\ell,k,[s]}^{SF,D} \geq \lambda_{\ell,k,[s]}^{SF,D}, \quad \forall \ell, \forall k \in \mathcal{K}_D, \forall s,$

$$(C15a) : \bar{q}_{\ell,k}^{M,[n_M]} + \lambda_{\ell,k}^{M,[n_M]} - T_M r_{\ell,k}^{M,[n_M]} \leq \bar{q}_{\ell,k}^{M,[n_M+1]}, \quad \forall(\ell, k, n_M),$$

$$(C15b) : 0 \leq \bar{q}_{\ell,k}^{M,[n_M]}, \quad \sum_{\forall k \in \mathcal{K}_M} \bar{q}_{\ell,k}^{M,[n_M]} \leq q_{\ell}^{M,\text{max}}, \quad \forall(\ell, n_M),$$

$$(C16a) : \bar{q}_{0,k}^{X,[n_X]} + \lambda_{0,k}^{X,[n_X]} - T_X r_{0,k}^{X,[n_X]} \leq \bar{q}_{0,k}^{X,[n_X+1]}, \quad \forall(k, n_X), \forall x \in \{M, S\},$$

$$(C16b) : 0 \leq \bar{q}_{0,k}^{X,[n_X]}, \quad \sum_{\forall k \in \mathcal{K}_X} \bar{q}_{0,k}^{X,[n_X]} \leq q_0^{X,\text{max}}, \quad \forall n_X, \forall x \in \{M, S\},$$

where $r_{\ell,k}^{M,[n_M]} = \sum_{\forall v_M} r_{\ell,k}^{M,[v_M,n_M]}, r_{0,k}^{X,[n_X]} = \sum_{\forall v_X} r_{0,k}^{X,[v_X,n_X]}$ while $r_{\ell,k}^{M,[v_M,n_M]}, r_{\ell,k}^{SF,D}, r_{0,k}^{X,[v_X,n_X]}$ satisfy constraints

$$(C17.1) : R_{\ell,k}^{M,[v_M,n_M]}(\mathbf{P}_c) \geq r_{\ell,k}^{M,[v_M,n_M]}, \quad \forall(\ell, v_M, n_M), \forall k \in \mathcal{K}_M,$$

$$(C17.2) : R_{\ell,k,[s]}^{SF,D}(\mathbf{P}_c) \geq r_{\ell,k,[s]}^{SF,D}, \quad \forall \ell, \forall k \in \mathcal{K}_D, \forall s,$$

$$(C18) : r_{0,k}^{X,[v_X,n_X]}(\mathbf{P}_c) \geq r_{0,k}^{X,[v_X,n_X]}, \quad \forall k \in \mathcal{K}_X \quad \forall(v_X, n_X), \forall x \in \{M, S\},$$

Therefore, problem $(\mathcal{P}_0)_c$ can be rewritten as

$$(\mathcal{P}_1)_c : \min_{\bar{\omega}_c, \mathbf{P}_c, \bar{q}_c, \mathbf{r}_c} f_{\text{obj}}(\bar{q}_c) \text{ s.t. (C1)–(C3), (C5), (C6), (C8), (C9), (C10), (C11), (C12), (C14)–(C16), (C17), (C18).}$$

Obviously, problem (\mathcal{P}_1) is still non-convex due to the non-convexity of SINR and rate constraints (C10), (C17), (C18).

3) *Convexify SINR and Rate Constraints:* These constraints can be convexified by the following propositions.

Proposition 1. *Constraints (C17.1), (C18) are convexified as*

$$(\tilde{C}17a) : w_M F_{\ell,k}^{R,M,[v_M,n_M]}(\mathbf{P}_c, \eta_c) \geq r_{\ell,k}^{M,[v_M,n_M]},$$

$$(\tilde{C}17b) : \Psi_{\ell,k}^{TN,[v_M,n_M]}(\mathbf{P}_c) + \Theta_k^{TN,[v_M,n_M]}(\mathbf{P}_c) + \sigma_{M,k}^2 \leq F_{\text{exp}}^{(i)}(\eta_{\ell,k}^{[v_M,n_M]}),$$

$$(\tilde{C}18a) : w_M F_{0,k}^{R,M,[v_M,n_M]}(\mathbf{P}_c, \eta_c) \geq r_{0,k}^{M,[v_M,n_M]},$$

$$(\tilde{C}18b) : \Theta_k^{\text{Sat},M,[v_M,n_M]}(\mathbf{P}_c) + \sigma_{M,k}^2 \leq \mathcal{F}_{\text{exp}}^{(i)}(\eta_{0,k}^{[v_M,n_M]}),$$

$$(\tilde{C}18c) : R_{0,k}^{S,[v_S,n_S]}(\mathbf{P}_c) \geq R_{0,k}^{S,[v_S,n_S]},$$

with $\mathcal{F}_{\text{exp}}^{(i)}(u) \triangleq \exp(u^{(i)})(u - u^{(i)} + 1)$, $F_{\ell,k}^{R,M,[v_M,n_M]}(\mathbf{P}_c, \eta_c) \triangleq \log_2(p_{\ell,k}^{[v_M,n_M]} h_{\ell,k}^{[v_M,n_M]} + \Psi_{\ell,k}^{M,[v_M,n_M]}(\mathbf{P}_c) + \Theta_k^{TN,[v_M,n_M]}(\mathbf{P}_c) + \sigma_{M,k}^2) - \eta_{\ell,k}^{[v_M,n_M]} / \ln(2)$, and $F_{0,k}^{R,M,[v_M,n_M]}(\mathbf{P}_c, \eta_c) \triangleq \log_2(p_{0,k}^{[v_M,n_M]} g_k^{[v_M,n_M]} + \Theta_k^{\text{Sat},[v_M,n_M]}(\mathbf{P}_c) + \sigma_{M,k}^2) - \eta_{0,k}^{[v_M,n_M]} / \ln(2)$; and $\eta_c = \{\eta_{0,k}^{[v_M,n_M]}, \eta_{\ell,k}^{[v_X,n_X]} | \forall(\ell, k, v_X, n_X), \forall x \in \{D, M\}\}$ is a slack variable.

Proof: Please see appendix A. ■

The SINR constraint (C11) and rate constraint (C17.2) for D services can be convexified by the following proposition.

Proposition 2. *Constraint (C10) can be convexified as*

$$(\tilde{C}10a) : F_{\ell,k}^{R,D,[v_D,n_D]}(\mathbf{P}_c, \eta_c) \geq \mathcal{F}_{\text{apx}}^{(i)}(p_{\ell,k}^{[v_D,n_D]}) \log_2(1 + \gamma_0^D),$$

$$(\tilde{C}10b) : \Psi_{\ell,k}^{[v_D,n_D]}(\mathbf{P}_c) + \sigma_{D,k}^2 \leq \mathcal{F}_{\text{exp}}^{(i)}(\eta_{\ell,k}^{[v_D,n_D]}),$$

with $F_{\ell,k}^{R,D,[v_D,n_D]}(\mathbf{P}_c, \eta_c) = \log_2(p_{\ell,k}^{[v_D,n_D]} h_{\ell,k}^{[v_D,n_D]} + \Psi_{\ell,k}^{[v_D,n_D]}(\mathbf{P}_c) + \sigma_{D,k}^2) - \eta_{\ell,k}^{[v_D,n_D]} / \ln(2)$.

Proof: Please see appendix B. ■

Proposition 3. Constraint (C17.2) can be convexified as

$$(\tilde{C}17c): w_D \sum_{\forall (v_D, n_D)} F_{\ell, k}^{R, D, [v_D, n_D]} (\mathbf{P}_c, \boldsymbol{\eta}_c) - \chi_D \mathcal{F}_{\text{sqrt}}^{(i)} (\zeta_{\ell, k, [s]}) \geq r_{\ell, k, [s]}^{\text{SF, D}},$$

$$(\tilde{C}17d): \zeta_{\ell, k, [s]} \geq \sum_{\forall (v_X, n_X)} \mathcal{F}_{\text{apx}}^{(i)} (p_{\ell, k}^{[v_D, n_D]}),$$

where $\mathcal{F}_{\text{sqrt}}^{(i)}(x) \triangleq x / (2\sqrt{x^{(i)}}) + \sqrt{x^{(i)}}/2$ and $\zeta_c \triangleq \{\zeta_{\ell, k, [s]} | \forall \ell, \forall k \in \mathcal{K}_D, \forall s \in \mathcal{T}_{\text{SF}}^{\text{C}, c}\}$ is a slack variable.

Proof: See appendix C. \blacksquare

Thanks to proposition 1, 2, and 3 problem $(\mathcal{P}_1)_c$ is transformed into the iterative convex problem $(\mathcal{P}_2)_c$ as

$$(\mathcal{P}_2)_c : \min_{\omega_c, \mathbf{P}_c, \bar{\mathbf{q}}_c, \mathbf{r}_c, \boldsymbol{\eta}_c, \boldsymbol{\zeta}_c} f_{\text{obj}} (\bar{\mathbf{q}}_c) \text{ s.t. } (\tilde{C}1) - (\tilde{C}3), (\tilde{C}5), (\tilde{C}6), (\tilde{C}8) - (\tilde{C}10), (\mathcal{C}11), (\mathcal{C}12), (\tilde{C}13) - (\tilde{C}18),$$

Using outcome of solving $(\mathcal{P}_2)_c$, $\boldsymbol{\alpha}_c$ and $\boldsymbol{\beta}_c$ are recovered as

$$\alpha_{\ell, k}^{[v_X, n_X]} = 1 \text{ if } p_{\ell, k}^{[v_X, n_X]} \geq \epsilon; \alpha_{\ell, k}^{[v_X, n_X]} = 0 \text{ otherwise,} \quad (36a)$$

$$\beta_k^{[v_X, n_X]} = 1 \text{ if } p_{0, k}^{[v_X, n_X]} \geq \epsilon; \beta_k^{[v_X, n_X]} = 0 \text{ otherwise.} \quad (36b)$$

The BWA variable \mathbf{b}_c is recovered by (30). The proposed solution “DT-JointRA” to solve problem $(\mathcal{P}_0)_c$ using predicted information $\{\hat{\mathbf{h}}_c, \hat{\mathbf{g}}_c, \hat{\boldsymbol{\lambda}}_c\}$ is summarized in Alg. 2.

Proposition 4. Alg. 2 is guaranteed to converge to a local optimal solution of problem $(\mathcal{P}_0)_c$.

Proof: Proposition 4 can be proved similarly as proposition 4 in [16]. Particularly, due to the properties of the SCA-based problem [31] and limited transmit power, the generated objective value sequence by solving $(\mathcal{P}_2)_c$ is non-increasing and bounded, resulting in Alg. 2’s convergence. In additional, by recovering binary variables, the feasible set of $(\mathcal{P}_2)_c$ is a subset of that of $(\mathcal{P}_0)_c$. Hence, Alg. 2 converges to a local optimal solution of $(\mathcal{P}_0)_c$. \blacksquare

C. RT-Refine Solution

Problems $(\mathcal{P}_0^{\text{refi}})_s$ and $(\mathcal{P}_0)_c$ share a similar structure with certain omitted constraints and variables in $(\mathcal{P}_0^{\text{refi}})_s$. Hence, by using approximation steps for $(\mathcal{P}_0)_c$, $(\mathcal{P}_0^{\text{refi}})_s$ is transformed into iterative convex problem $(\mathcal{P}_1^{\text{refi}})_s$ as

$$(\mathcal{P}_1^{\text{refi}})_s : \min_{\mathbf{p}[s], \mathbf{r}[s], \boldsymbol{\eta}[s], \bar{\mathbf{q}}[s]} f_{\text{obj}} (\bar{\mathbf{q}}[s]) \text{ s.t. } (\tilde{C}5)_s, (\tilde{C}6)_s, (\tilde{C}9)_s, (\tilde{C}10)_s, (\mathcal{C}11)_s, (\tilde{C}14)_s, (\tilde{C}15)_s, (\tilde{C}16)_s, (\tilde{C}17)'_s, (\tilde{C}18a, b)'_s$$

where $(\tilde{C}17)'$, $(\tilde{C}18a)'$, and $(\tilde{C}18b)'$ are the convex constraint revised from $(\tilde{C}17)$, $(\tilde{C}18a)$, and $(\tilde{C}18b)$ using terms $\hat{\Theta}_k^{\text{TN}, [v_M, n_M]}$ and $\hat{\Theta}_k^{\text{Sat}, [v_M, n_M]}$ instead of $\Theta_k^{\text{TN}, [v_M, n_M]}$ and $\Theta_k^{\text{Sat}, [v_M, n_M]}$, respectively. It is worth noting that information $\{\hat{\mathbf{h}}_e^*, \hat{\mathbf{g}}_e, \boldsymbol{\lambda}_e\}$ is used to solve $(\mathcal{P}_1^{\text{refi}})_s$. The overall solution of RT-Refine Algorithm, is described in Alg. 3, with the workflow illustrated in Fig. 6.

Proposition 5. Alg. 3 converges to a local optimal solution of problem sequence $\{(\mathcal{P}_0^{\text{refi}})_s\}_{\forall s}$.

Proof: For each cycle c , Alg. 3 solves $(\mathcal{P}_2)_c$ and $(\mathcal{P}_1^{\text{refi}})_s$. Solving $(\mathcal{P}_2)_c$ and $(\mathcal{P}_1^{\text{refi}})_s$ are ensured to converge since they are the SCA-based problems [31]. Besides, for each loop of SF s (steps 8 – 16), the $(\mathcal{P}_1^{\text{refi}})_s$ ’s feasible set is a subset of that of $(\mathcal{P}_0^{\text{refi}})_s$. Hence, Alg. 3 converges to a local optimal solution of $\{(\mathcal{P}_0^{\text{refi}})_s\}_{\forall s}$. \blacksquare

Algorithm 2 DT-BASED JOINT-RA ALGORITHM (DT-JOINTRA)

- Input:** Predicted $\{\hat{\mathbf{h}}_c, \hat{\mathbf{g}}_c, \hat{\boldsymbol{\lambda}}_c\}$ from DT.
- Set $i = 1$ and generate an initial point $(\mathbf{P}_c^{(0)}, \boldsymbol{\eta}_c^{(0)}, \boldsymbol{\zeta}_c^{(0)})$.
- repeat**
- Solve problem $(\mathcal{P}_2)_c$ to obtain $(\mathbf{P}_c^*, \boldsymbol{\eta}_c^*, \boldsymbol{\zeta}_c^*)$.
- Update $(\mathbf{P}_c^{(i)}, \boldsymbol{\eta}_c^{(i)}, \boldsymbol{\zeta}_c^{(i)}) = (\mathbf{P}_c^*, \boldsymbol{\eta}_c^*, \boldsymbol{\zeta}_c^*)$ and $i := i + 1$.
- until** Convergence
- Recovery $\boldsymbol{\omega}_c^*$ and binary solutions \mathbf{b}_c^* , $\boldsymbol{\alpha}_c^*$, and $\boldsymbol{\beta}_c^*$ by (34), (30), and (36).
- Output:** Solution $\{\mathbf{b}_c^*, \boldsymbol{\omega}_c^*, \mathbf{P}_c^*, \boldsymbol{\alpha}_c^*, \boldsymbol{\beta}_c^*, \boldsymbol{\eta}_c^*\}$ for cycle c .

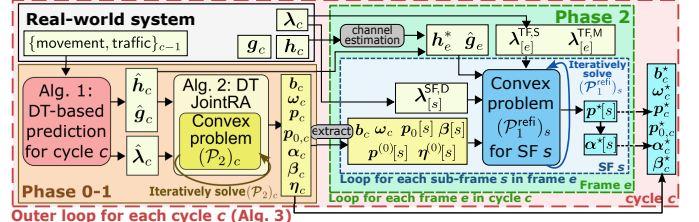


Fig. 6: Flowchart of the proposed DT-based algorithm.

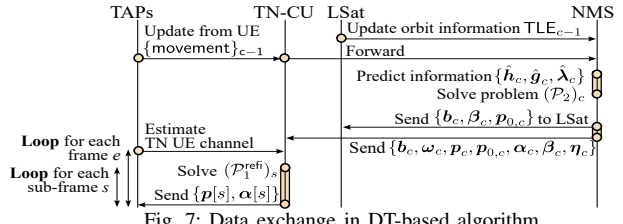


Fig. 7: Data exchange in DT-based algorithm.

D. RT-Refine Algorithm Implementation

Regarding implementation, Fig. 7 shows execution steps and data exchange among TAPs, TCU, LSat, and NMS in the RT-Refine algorithm. The procedure is summarized as

- At each cycle, TAPs and LSat send the updated UE movement and orbit information to NMS. Based on which, the necessary information is predicted and Alg. 2 is executed to pre-solve $(\mathcal{P}_2)_c$ for upcoming cycle c .
- Once $(\mathcal{P}_2)_c$ is solved, all outcomes are sent to TCU for the next phase, while only SatNet’s BWA, power control, and UE/RB assignment solutions are sent to LSat.
- For the given solution sent from NMS, TCU refines TN short-term decisions at each SF s . Subsequently, solutions are sent to TAPs.

One can see that, at each cycle, there is only one round-trip communication between LSat and ground segments, i.e., LSat updates orbit information and then NMS sends transmission solutions. Additionally, depending on the stability and accuracy of orbit information (TLE data), LSat can update less frequently, which further reduces costly signaling. The complexity aspect is further discussed in the following section.

V. BENCHMARKS AND COMPLEXITY ANALYSIS

This section provides several benchmarks for comparison purposes. Due to space limit, we describe the overall big-O complexity instead of a detailed analysis where those of solving convex problems are derived by [32].

A. Greedy Algorithm

The **Greedy Algorithm** is summarized in Alg. 4. The number of used SCs for D services is fixed to N_{SC}^D while BW for the M and S services is uniformly allocated. The AP/LSat-UE association and RB assignment are selected based on channel gain matrices in cycle c . Afterward, the water-filling algorithm is utilized for power allocation by ignoring interference with ϵ_{pow} tolerance for water level searching. The traffic steering decision is set proportional to the UE rate. One

Algorithm 3 REAL-TIME-REFINE ALGORITHM (RT-REFINE)

```

1: Initialize: Actual information  $\{\lambda_0, \mathbf{u}_0^{\text{ue}}, \text{TLE}_0\}$  in cycle 0.
2: for Each cycle  $c$ ,  $c = 1 \rightarrow N_{\text{CY}}$  do
3:   Phase 0: Predict  $\{\hat{\mathbf{h}}_c, \hat{\mathbf{g}}_c, \hat{\lambda}_c\}$  by Alg. 1.
4:   Phase 1: Execute Alg. 2 for solution  $\{\mathbf{b}_c^*, \omega_c^*, \mathbf{P}_c^*, \alpha_c^*, \beta_c^*, \eta_c^*\}$  for cycle  $c$ .
5:   Phase 2: Re-optimize using  $\mathbf{h}_e^*, \hat{\mathbf{g}}_e, \lambda_e$  and initial point from output in step 4.
6:   for Each frame  $e$  in cycle  $c$  do
7:     Collect  $\{\lambda_e^{\text{TF},x}\}, x \in \{\text{M}, \text{S}\}$ . Estimate channel of TN UEs and build  $\mathbf{h}_e^*$ .
8:     for Each SF  $s$  in frame  $e$  do
9:       Collect  $\lambda_s^{\text{SF},\text{D}}$ , set  $i=0$  and extract initial point from solution in step 4.
10:      repeat
11:        Solve problem  $(\mathcal{P}_1^{\text{refi}})_s$  to obtain  $(\mathbf{p}^*[s], \eta^*[s])$ .
12:        Update  $(\mathbf{p}^{(i)}[s], \eta^{(i)}[s]) = (\mathbf{p}^*[s], \eta^*[s])$  and  $i := i + 1$ .
13:      until Convergence
14:      Recover binary variable  $\alpha^*[s]$  by (36).
15:      Output SF  $s$ : The adjusted solution  $(\mathbf{p}^*[s], \alpha^*[s])$ .
16:    end for
17:  end for
18:  Output cycle  $c$ : Solution  $\{\mathbf{b}_c^*, \omega_c^*, \mathbf{P}_c^*, \mathbf{P}_{0,c}^*, \alpha_c^*, \beta_c^*\}$  with adjusted  $(\mathbf{p}_c^*, \alpha_c^*)$ .
19: end for
20: Output: Solution for  $N_{\text{CY}}$  cycles.

```

TABLE II: QL and the remaining traffic D of Heuristic algorithm versus N_{SC}^{D} .

Num. SCs for D services, N_{SC}^{D}	1	2	3	4	5
Mean QL (MB)	20.12	23.12	27.08	31.55	37.29
Remaining D traffic (%)	22.2	19.5	18.4	17.8	17.4

notes that this algorithm does not guarantee SINR/rate and QL constraints (C10), (C14) – (C16).

B. Heuristic Algorithm

A **Heuristic Algorithm** is further proposed by updating the greedy algorithm above, where the BWA is adopted from [25]. In particular, the approach is developed from Alg. 4 as: **step 1**) traffic λ_c is added to input; **step 4**) BW for the M and S services is set proportional to the remaining QL in cycle $(c-1)$; **step 19**) after power control, the remaining QL is computed based on the rate of UE and traffic. The complexity of the greedy (Alg. 4) and heuristic algorithms is

$$X_{\text{Grd-Heu}} = O(N_{\text{CY}}(X_{\text{Assoc}} - N \log_2(\epsilon_{\text{pow}}))). \quad (37)$$

C. Other Benchmark

Given the similar aspects with our work, the proposed algorithm in [25] is reused with modifications to adapt to our considered problem. Particularly, for the long-term decisions, BWA for BWPs is set proportional to the next cycle service traffics while the traffic steering for each node is set proportional to the previous cycle sum-rate of that node. For the short-term decision, power control and RB assignment are jointly optimized wherein the co-channel interference is ignored [25]. The adapted algorithm using full actual information is called as **Reference Algorithm** with a complexity of

$$X_{\text{RefAlg}} = O(N_{\text{CY}}N_{\text{iter}}a_{\text{DTJRA}}^2(a_{\text{RefAlg}} + b_{\text{RefAlg}})b_{\text{RefAlg}}^{1/2}), \quad (38)$$

where $a_{\text{RefAlg}} = N_{\text{SF}}(L(K_D(8\bar{V}_D + 2) + K_M(6\bar{V}_M + 2)) + K_M(6\bar{V}_M + 2) + K_S(3\bar{V}_S + 1))$, $b_{\text{RefAlg}} = N_{\text{SF}}(L(K_D(8\bar{V}_D + 3) + K_M(\bar{V}_M + 1) + 2(2\bar{V}_D + \bar{V}_M + 3)) + 2(2K_D\bar{V}_D + K_M(3\bar{V}_M + 2)) + 2\bar{V}_M + K_S(\bar{V}_S + 2) + \bar{V}_S + 5)$, and N_{iter} is the number of iterations for convergence.

In addition, a **Full Information Algorithm (FIA)** is further examined where DT-JointRA algorithm is executed with full actual information.

D. Proposed Algorithm Complexity

According to Alg. 2 and , the complexities of DT-JointRA and RT-Refine algorithms are expressed respectively as [32]

$$X_{\text{DTJRA}} = O(N_{\text{CY}}N_{\text{iter}}a_{\text{DTJRA}}^2(a_{\text{DTJRA}} + b_{\text{DTJRA}})b_{\text{DTJRA}}^{1/2}), \quad (39)$$

$$X_{\text{RTRefi}} = X_{\text{DTJRA}} + O(N_{\text{CY}}N_{\text{SF}}\bar{N}_{\text{iter}}a_{\text{RTRefi}}^2(a_{\text{RTRefi}} + b_{\text{RTRefi}})b_{\text{RTRefi}}^{1/2}), \quad (40)$$

Algorithm 4 GREEDY ALGORITHM

```

1: Input: Channel  $\mathbf{h}_c = [h^x(\ell, k, v_x, n_x)]$ ,  $\mathbf{g}_c = [g^x(k, v_x, n_x)]$ ,  $\forall (\ell, k, v_x, n_x, x, c)$ .
2: Initialize: Zero matrices  $\alpha_c$ ,  $\beta_c$ , and  $\mathbf{b}_c$  with  $\forall c$ .
3: for Each cycle  $c$  do
4:   Use  $N_{\text{sb}}^{\text{d}}$  D SCs, uniformly allocate BW for services  $x \in \{\text{M}, \text{S}\}$ . Build  $\mathbf{b}_c$ .
5:   for Each frame  $e$  do
6:     Extract  $\{\mathbf{h}_e, \mathbf{g}_e, \alpha_e, \beta_e\}$  for frame  $e$ . Set elements of non-using SCs to zero.
7:     for Each UE  $k$  service  $x$  do
8:       while  $\mathbf{h}_e^x(:, k, :, :) \neq 0$  do
9:         Find index  $(\hat{\ell}, \hat{v}, \hat{n})$  where  $\mathbf{h}_e^x(\hat{\ell}, k, \hat{v}, \hat{n}) = \max(\mathbf{h}_e^x(:, k, :, :))$ .
10:        Set  $\alpha_e^x(\hat{\ell}, k, \hat{v}, \hat{n}) = 1$ ,  $\mathbf{h}_e^x(:, k, \hat{v}, \hat{n}) = 0$  and  $\mathbf{h}_e^x(\hat{\ell}, :, \hat{v}, \hat{n}) = 0$ .
11:       end while
12:       while  $\mathbf{g}_e^x(k, :, :) \neq 0$  do
13:         Find index  $(\hat{v}, \hat{n})$  satisfying  $\mathbf{g}_e^x(k, \hat{v}, \hat{n}) = \max(\mathbf{g}_e^x(k, :, :))$ .
14:         Set  $\beta_e^x(\hat{v}, \hat{n}) = 1$  and  $\mathbf{g}_e^x(:, \hat{v}, \hat{n}) = 0$ .
15:       end while
16:     end for
17:   end for
18:   Assign  $\alpha_c, \beta_c$  to  $\alpha_c, \beta_c$ 
19:   Power control  $\{\mathbf{P}_c\}$ : using water-filling scheme by ignoring interference.
20:   Traffic steering  $\omega_c$ : set proportional to UE rate.
21: end for
22: Output: Solution  $\{\mathbf{b}_c, \omega_c, \mathbf{P}_c, \alpha_c, \beta_c\}$ ,  $\forall c$  for  $N_{\text{CY}}$  cycles.

```

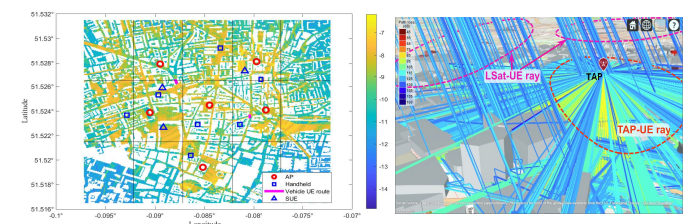


Fig. 8: Simulation scenario, TN channel heatmap (log10 scale), and RayT. where N_{iter} and \bar{N}_{iter} are the iteration numbers for convergence in solving $(\mathcal{P}_2)_c$ and $(\mathcal{P}_1^{\text{refi}})_s$. $a_{\text{DTJRA}} = N_{\text{SF}}(L(K_D(8\bar{V}_D + 2) + K_M(6\bar{V}_M + 2)) + K_M(6\bar{V}_M + 2) + K_S(3\bar{V}_S + 1)) + L(\bar{V}_D + \bar{V}_M)$, $b_{\text{DTJRA}} = N_{\text{SF}}(L(K_D(8\bar{V}_D + 3) + K_M(\bar{V}_M + 1) + 2(2\bar{V}_D + \bar{V}_M + 3)) + 2(2K_D\bar{V}_D + K_M(3\bar{V}_M + 2)) + 2\bar{V}_M + K_S(\bar{V}_S + 2) + \bar{V}_S + 5) + \bar{V}_D + \bar{V}_M + 1$, $a_{\text{RTRefi}} = L(K_D(8\bar{V}_D + 2) + K_M(6\bar{V}_M + 2)) + K_M(4\bar{V}_M + 2)$, $b_{\text{RTRefi}} = L(K_D(8\bar{V}_D + 3) + K_M(\bar{V}_M + 1) + 2(2\bar{V}_D + \bar{V}_M + 3)) + 2(2K_D\bar{V}_D + K_M(3\bar{V}_M + 2)) + 1$.

VI. NUMERICAL RESULTS**A. Simulation Setup**

The simulation is conducted with 3D map in an area of 3km^2 at $(51.524^\circ\text{N}, 0.085^\circ\text{W})$ in London city. For simulation data, the vehicular UE route and LSat orbit are taken from Google Navigator and Starlink LEO TLE, the arrival traffic is taken from an actual dataset [33]. Environment channels are generated using the DT model with coefficient $\xi = 0.5$.

The key simulation parameters are: system BW $W^{\text{tot}} = 15$ MHz, operation frequency $f_c = 3.4$ GHz, LSat altitude 500 km, antenna parameters of AP, LSat, SUE as in [34], [35], vehicle UE antenna and RayT parameters as in [16], [36], number of cycles $N_{\text{CY}} = 20$, number of frames/cycle $N_{\text{TF}} = 5$, numbers of TAPs, UEs (N, K_D, K_M, K_S) = $(6, 4, 5, 3)$, power budget at AP and LSat ($p_{\text{AP}}^{\text{max}}, p_{\text{LSat}}^{\text{max}}$) = $(34, 36)$ dBm, maximum QL $q_{\ell}^{\text{m},\text{max}} = q_0^{\text{x},\text{max}} = 2$ MB, interference margin for the RT-Refine algorithm $\kappa = 1.1$. For intuition, the simulation scenario with UE position and channel gain heatmap, and RayT result are shown in Fig. 8. For heuristic algorithms, the mean QL and remaining D traffic versus N_{SC}^{D} are shown in Table. II. To minimize the congestion, we select $N_{\text{SC}}^{\text{D}} = 1$.

Fig. 9 shows the convergence of QL in two phases due to the proposed algorithms in different cases. It is worth noting that the RT-Refine algorithm consists of phase 1-the DT-JointRA

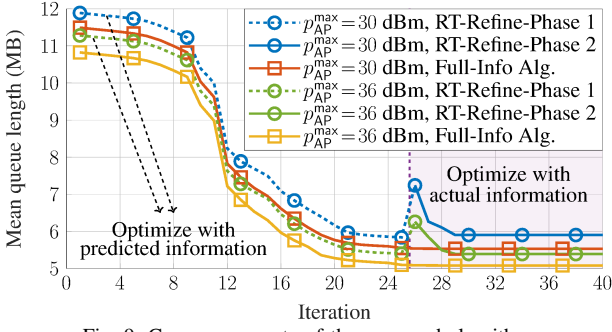
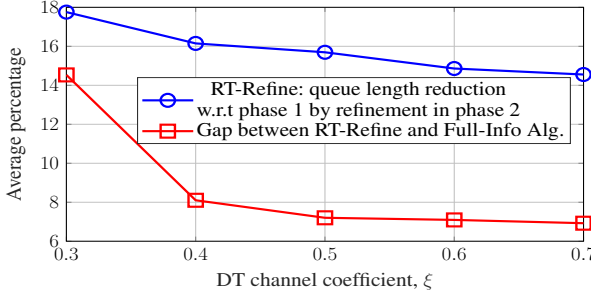


Fig. 9: Convergence rate of the proposed algorithms.

Fig. 10: QL versus DT channel coefficient, ξ .

algorithm and phase 2—the refinement stage, which operate on different input types, i.e., predicted and actual information, respectively. Since the DT-JointRA algorithm and FIA share the same structure with only differences in inputs, their convergence rates are similar. Particularly, the DT-JointRA algorithm and FIA require only about 25 iterations for convergence in both cases $p_{AP}^{\max} = 30$ dBm and $p_{AP}^{\max} = 36$ dBm. Although in the RT-Refine algorithm, phase 2 is executed right after phase 1 (i.e., DT-JointRA), it is bumpy at the beginning of phase 2, which is due to the changes in inputs, i.e., replacing $\{\hat{\mathbf{h}}_e, \hat{\lambda}_e\}$ by $\{\mathbf{h}_e^*, \lambda_e\}$. However, phase 2 requires only about 3 iterations for convergence. This emphasizes the practical implementation aspect of the proposed RT-Refine algorithm.

Regarding the impact of DT channel coefficient ξ on the performance of the proposed RT-Refine algorithm, Fig. 10 illustrates the QL improvement of re-optimization in phase 2 of the RT-Refine algorithm and the QL gap between the RT-Refine algorithm and FIA. Based on the channel model in Section II-C, one can see that a larger ξ results in a smaller difference between the emulated real environment and its DT reduces. Hence, both lines decrease as ξ increases. Particularly, at $\xi = 0.3$, $\xi = 0.5$, and $\xi = 0.7$, re-optimizing in phase 2 can reduce the QL by about 17.7%, 15.7%, and 14.5% compared to DT-JointRA outcomes, and the percentage gaps between the RT-Refine algorithm and FIA are about 14.5%, 7.3%, and 6.9% compared to FIA outcomes, respectively.

Fig. 11 depicts the mean QL versus interference margin κ in the RT-Refine algorithm. One can see that the mean QL outcome first decreases and then increases as κ increases. Particularly, the mean QL at $\kappa = (1, 1.1, 1.2, 1.3)$ is about (3.59, 3.51, 3.53, 3.63) MB. This phenomenon can be explained as follows. First, one notes that in phase 2 of the RT-Refine algorithm, only actual channels from TAPs to their own served UEs are used while other channels are kept as predicted ones. For $\kappa = 1$, the prediction error in these interference channels is not accounted for. In contrast, for

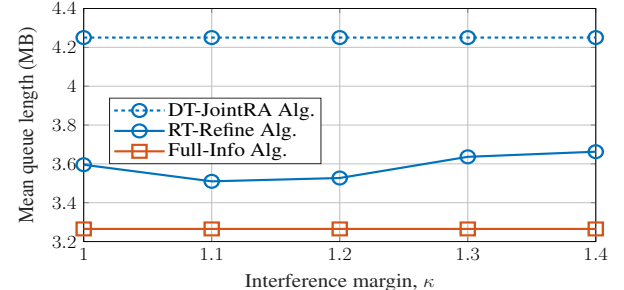


Fig. 11: QL versus margin interference.

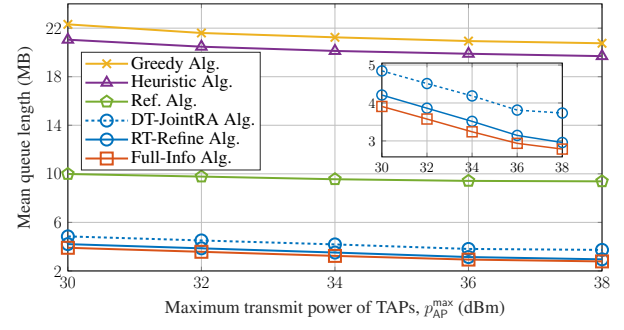


Fig. 12: QL versus TAP power budget.

$\kappa > 1$, the prediction uncertainty is considered, promoting TAPs to reduce their transmit power to protect UEs served by LSat. Hence, at higher κ , e.g., at $\kappa = 1.1$ and $\kappa = 1.2$, mean QL decreases. However, for sufficiently high κ , the prediction error is overestimated, leading the TAPs to reduce transmit power more than necessary, which results in rate degradation and an increase in QL. By appropriately choosing this margin, i.e., $\kappa = 1.1$, re-optimization in phase 2 can reduce about 0.75 MB in mean QL, and the gap between the RT-Refine and FIA lines is only about 0.25 MB. This result demonstrates the effectiveness of considering this margin against interference channel prediction errors while avoiding costly channel estimation. Based on this result, margin $\kappa = 1.1$ is selected for the remaining simulations.

Fig. 12 shows the mean QL outcomes of proposed algorithms and benchmarks versus the AP power budget. Regarding the greedy and heuristic benchmarks, the mean QL gap between two lines is about 1.12 MB which is due to the adaptive BWA based on the remaining QL of the heuristic algorithm. Moreover, thanks to the joint user association, RB assignment, and power control optimization, the reference algorithm further reduces mean QL approximately 10–11 MB. However, compared to the proposed algorithms, since benchmarks ignore interference, the QL performance gap between the proposed and benchmark algorithms is significant, i.e., about 17 MB compared with greedy/heuristic algorithms and about 5–5.7 MB compared with reference algorithm. Additionally, the proposed algorithms satisfy D service requirements in all considered cases while the unserved D traffics of the heuristic and reference algorithms are about 22.2% and 17.5%, respectively. Regarding proposed algorithms, the gap between the DT-JointRA and RT-Refine lines, which indicates improvement by the refinement in RT-Refine-phase 2, is about 0.7 MB. Besides, compared to the proposed benchmark FIA which uses full actual information for optimization, the gap between the RT-Refine and FIA lines is only about 0.27 MB. Hence, in addition

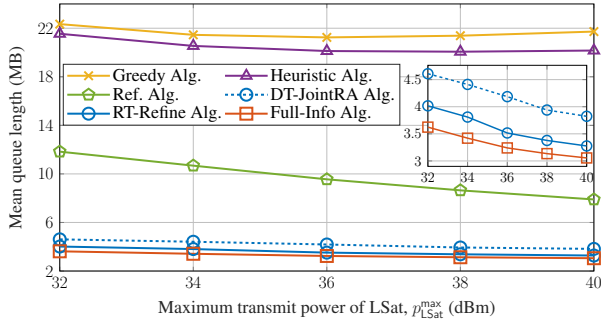


Fig. 13: QL versus LSat power budget.

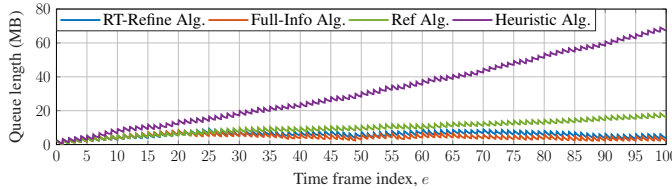


Fig. 14: QL over time of examined algorithms.

to superiority compared to two benchmarks, the proposed RT-Refine scheme shows the effectiveness of refining TAP power control to adjust solutions with the actual information at all considered cases of p_{AP}^{\max} . Additionally, a similar outcome trend of the proposed algorithms can be recognized. Particularly, with TAP power budget $p_{AP}^{\max} = 30 \rightarrow 36$ dBm, the mean QL decreases quickly, and with $p_{AP}^{\max} = 36 \rightarrow 38$ dBm, their decrease trend slightly reduces. While a higher power budget enables higher data rates, certain traffic flows can be fully served once the power budget reaches a sufficiently high level. This phenomenon shows that beyond $p_{AP}^{\max} = 36$ dBm, the power budget starts to be redundant for QL minimization.

Fig. 13 depicts the mean QL performance of the examined schemes with different LSat power budgets. Regarding the greedy and heuristic benchmarks, one can see that the mean QL outcomes first decrease and then increase. This is due to the impact of interference caused by LSat in the whole coverage area is not addressed in the power control phase. Similar to results in Fig. 12, the adaptive BWA in the heuristic scheme brings the improvement in terms of QL compared to the greedy one while the joint user association, RB assignment, and power control optimization in the reference one further reduce mean QL. However, compared to the proposed algorithms, the QL outcome gap is still significant. Regarding the proposed algorithms, a similar trend compared to results in Fig. 12 can be recognized. Particularly, the QL outcomes linearly decrease as LSat power budget p_{LSat}^{\max} increases, while the decreasing trend slightly reduces with $p_{LSat}^{\max} = 36 \rightarrow 40$ dBm. This slight degradation indicates that the LSat power budget starts to be redundant for QL minimization.

For insights into QL minimization performance, Fig. 14 illustrates the QL evolution of FIA, RT-Refine, the heuristic method, and the reference algorithm over time (frames). The heuristic benchmark exhibits a rapidly and almost linearly increasing QL, resulting in a significantly higher average QL than the proposed and reference schemes. Although the reference algorithm achieves a lower QL, it remains unstable as its QL continues to grow over time. In contrast, the proposed algorithms not only provide substantially better QL performance but also maintain the QL consistently below ap-

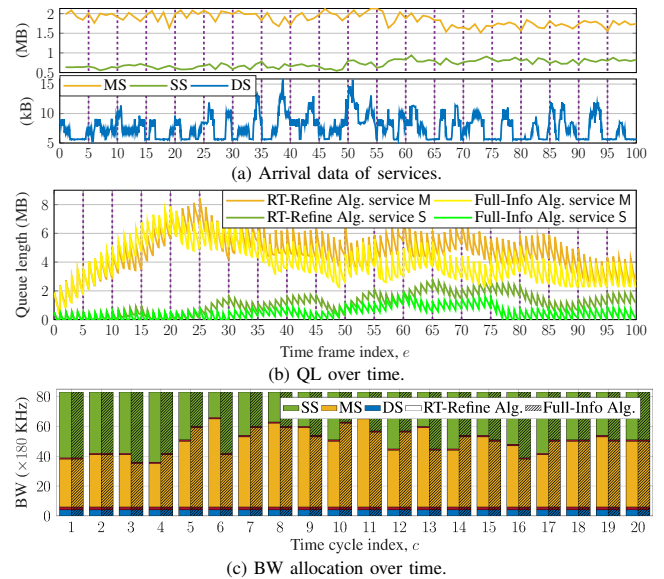


Fig. 15: Arrival data, QL, and BWA over time.

proximately 10 MB across frames. These results demonstrate the superiority of the proposed solutions in terms of both QL minimization and long-term stability.

For more insight into the QL over time, Fig. 15 shows the arrival data of services, QL and BWA outcomes over time of the RT-Refine algorithm and FIA. Although the arrival data of D services is quite small, i.e., only about 5–10 kB/frame, it is not completely served by using benchmarks since the interference is ignored. However, the proposed algorithms can satisfy D service requirements by allocating only 1 SC for BWP D. Besides, due to the larger varying total arrival data size of the M and S services, the BWAs for these services change over cycles for QL minimization. One can see that, at each cycle, the BW is allocated adaptively based on the remaining QL in the previous cycle and the arrival data. Additionally, compared with the FIA benchmark using full actual information, the RT-Refine algorithm, which is proposed for implementation purposes, can provide a comparable performance in terms of QL minimization over time.

VII. CONCLUSION

This work studied the novel DT-aided joint spectrum sharing, traffic steering, and resource allocation for ISTNs over time. The optimization problems aim to minimize the system congestion under system and service constraints. To assist RM, a digital-twin system is developed for information prediction. Based on this, we proposed a DT-JointRA algorithm implementable at the CNC to address the optimization problem. For practical implementation, a re-optimization phase is built on top of the DT-JointRA algorithm to refine its solution with the information in real-world systems. Through numerical results with the actual 3D map and traffic information, the proposed algorithms show the superiority in terms of congestion minimization, compared to benchmarks. Furthermore, the simulation results emphasize the practicality and effectiveness of the proposed algorithms in terms of adaptation ability.

APPENDIX A PROOF OF PROPOSITION 1

Consider function $f_r(x, y) = \log_2(1 + \frac{x}{y+a})$, $x, y \geq 0, a > 0$, constraint $f_r(x, y) \geq z$, $z \geq 0$ is approximated as [16]

$$\begin{cases} \log_2(x + y + a) \geq z + u/\ln(2), \\ y + a \leq f_{\text{exp}}^{(i)}(u) \triangleq \exp(u^{(i)})(u - u^{(i)} + 1), \end{cases} \quad (41)$$

where u and $u^{(i)}$ are the slack variable and its feasible point at iteration i , respectively. Apply approximation in (41) to log component in rate functions $R_{\ell,k}^{M,[v_M,n_M]}$ and $R_{0,k}^{M,[v_M,n_M]}$ with setting x , y , a , and u by the desired received power, the total interference terms, noise power, and the corresponding η , constraints (C17.1) and (C18) are convexified by $(\tilde{C}17a)$, $(\tilde{C}17b)$ and $(\tilde{C}18)$, respectively. Specifically, $R_{0,k}^{S,[v_S,n_S]}(\mathbf{P}_c)$ is concave, hence, constraint $(\tilde{C}20c)$ is convex.

APPENDIX B PROOF OF PROPOSITION 2

Constraint $(\tilde{C}10)$ is equivalently transformed as

$$\log_2(1 + \gamma_{\ell,k}^{D,[v_D,n_D]}(\mathbf{P}_c)) \geq \mathcal{F}_{\text{apx}}^{(i)}(p_{\ell,k}^{D,[v_D,n_D]}) \log_2(1 + \gamma_0^D), \quad (42)$$

$\forall(\ell, k, v_D, n_D)$. Apply approximation (41) to the log component by setting $x = p_{\ell,k}^{[v_D,n_D]} h_{\ell,k}^{[v_D,n_D]}$, $y = \Psi_{\ell,k}^{[v_D,n_D]}$, $a = \sigma_{D,k}^2$, and $u = \eta_{\ell,k}^{[v_D,n_D]}$, we obtain $(\tilde{C}10a)$ and $(\tilde{C}10b)$.

APPENDIX C PROOF OF PROPOSITION 3

Let $\zeta_{\ell,k,[s]}$ be the upper bound of the RB number allocated to $\text{AP}_\ell - \text{UE}_k^D$ link in SF s , constraint (C17.2) is rewritten as

$$w_D \sum_{\forall(v_D,n_D)} \log_2(1 + \gamma_{\ell,k}^{D,[v_D,n_D]}(\mathbf{P}_c)) - \chi_D \sqrt{\zeta_{\ell,k,[s]}} \geq r_{\ell,k,[s]}^{\text{SF},D}, \quad (43a)$$

$$\zeta_{\ell,k,[s]} \geq \sum_{\forall(v_D,n_D)} \|p_{\ell,k}^{[v_D,n_D]}\|_0. \quad (43b)$$

Apply approximation (32) to ℓ_0 -norm components, (43b) is convexified as $(\tilde{C}17d)$. In (43a), the log component can be convexified as in proposition 3 while the square root component is convexified as follows. Apply SCA technique, function $\mathcal{F}_{\text{sqrt}}(x) = \sqrt{x}$ is approximated at iteration i as

$$\mathcal{F}_{\text{sqrt}}(x) \leq x / (2\sqrt{x^{(i)}}) + \sqrt{x^{(i)}}/2 := \mathcal{F}_{\text{sqrt}}^{(i)}(x). \quad (44)$$

Use approximation (44) for sqrt term in (43a), we obtain the convex form as $(\tilde{C}17c)$.

REFERENCES

- H. Nguyen-Kha, V. N. Ha, T. Nguyen, E. Lagunas, S. Chatzinotas, and J. Grotz, "Dt-aided resource management in spectrum sharing integrated satellite-terrestrial networks," in *IEEE GLOBECOM*, 2025.
- C.-X. Wang *et al.*, "On the road to 6G: Visions, requirements, key technologies, and testbeds," *IEEE Commun. Surveys Tut.*, vol. 25, no. 2, pp. 905–974, Secondquarter 2023.
- ETSI, "Non-terrestrial networks, a native component of 6G: Vision on non-terrestrial networks in 6G system (or imt-2030)," 2024.
- FCC, "Single network future: Supplemental coverage from space," 2023.
- ESA, "Direct-to-device connectivity: An opportunity for europe," 2024.
- 3GPP, "Study on complementary reuse of terrestrial spectrum in satellite deployments," Tdoc RWS-230110, 2023, TSG RAN R19 Workshop.
- S. Communications, "Simplifying 5G with a network digital twin," 2019, white paper.
- H. X. Nguyen, R. Trestian, D. To, and M. Tatipamula, "Digital twin for 5g and beyond," *IEEE Commun. Mag.*, vol. 59, no. 2, pp. 10–15, 2021.
- M. Zhu *et al.*, "Toward real-time digital twins of em environments: Computational benchmark for ray launching software," *IEEE OJCOM*, vol. 5, pp. 6291–6302, 2024.
- J. Du, C. Jiang, H. Zhang, Y. Ren, and M. Guizani, "Auction design and analysis for SDN-based traffic offloading in hybrid satellite-terrestrial networks," *IEEE JSAC*, vol. 36, no. 10, pp. 2202–2217, Oct. 2018.
- Y. Zhang *et al.*, "Resource allocation in terrestrial-satellite-based next generation multiple access networks with interference cooperation," *IEEE J. Sel. Areas Commun.*, vol. 40, no. 4, pp. 1210–1221, Apr. 2022.
- H.-W. Lee, C.-C. Chen, S. Liao, A. Medles, D. Lin, I.-K. Fu, and H.-Y. Wei, "Interference mitigation for reverse spectrum sharing in B5G/6G satellite-terrestrial networks," *IEEE Trans. Veh. Technol.*, pp. 1–16, 2023.
- Z. Li, S. Han, M. Peng, C. Li, and W. Meng, "Dynamic multiple access based on RSMA and spectrum sharing for integrated satellite-terrestrial networks," *IEEE Trans. Wireless Commun.*, vol. 23, no. 6, 2024.
- H. Martikainen, M. Majamaa, and J. Puttonen, "Coordinated dynamic spectrum sharing between terrestrial and non-terrestrial networks in 5g and beyond," in *IEEE 24th Int. WoWMoM*, June 2023, pp. 419–424.
- J. Zhu, Y. Sun, and M. Peng, "Beam management in low earth orbit satellite communication with handover frequency control and satellite-terrestrial spectrum sharing," *IEEE Trans. Commun.*, pp. 1–1, 2024.
- H. Nguyen-Kha, V. Nguyen Ha, E. Lagunas, S. Chatzinotas, and J. Grotz, "Enhanced throughput and seamless handover solutions for urban 5g-vehicle c-band integrated satellite-terrestrial networks," *IEEE Trans. Commun.*, vol. 73, no. 11, pp. 12 836–12 853, 2025.
- D. Van Huynh and et al., "URLLC edge networks with joint optimal user association, task offloading and resource allocation: A digital twin approach," *IEEE Trans. Commun.*, vol. 70, no. 11, pp. 7669–7682, 2022.
- W. Sun, P. Wang, N. Xu, G. Wang, and Y. Zhang, "Dynamic digital twin and distributed incentives for resource allocation in aerial-assisted internet of vehicles," *IEEE IoT J.*, vol. 9, no. 8, pp. 5839–5852, 2022.
- Y. Gong, Y. Wei, Z. Feng, F. R. Yu, and Y. Zhang, "Resource allocation for integrated sensing and communication in digital twin enabled internet of vehicles," *IEEE Trans. Veh. Technol.*, vol. 72, no. 4, 2023.
- M. Wu, Y. Gao, Q. Song, K. Li, W. Lu, L. Guo, and A. Jamalipour, "Integrated resource collaboration for ris-assisted digital-twin-empowered internet of everything," *IEEE IoT J.*, vol. 12, pp. 23 275–23 287, 2025.
- H. Yu, Y. Liu, Z. Yang, H. Sun, and M. Chen, "Optimizing wireless resource management and synchronization in digital twin networks," *IEEE IoT J.*, vol. 12, no. 15, pp. 29 152–29 163, 2025.
- L. Tang *et al.*, "Dynamic slice resource management and information synchronization strategy in iot based on digital twin," *IEEE Trans. Intelligent Transportation Systems*, vol. 26, no. 5, pp. 6635–6650, 2025.
- H. Nguyen-Kha, V. N. Ha, E. Lagunas, S. Chatzinotas, and J. Grotz, "An experimental study of C-band channel model in integrated LEO satellite and terrestrial systems," in *Proc. MeditCom 2024*, 2024.
- Chee, Tommy and others, "D2.5 report on regulatory requirements: Spectrum policies and regulatory analysis," 2024, 6G-NTN project.
- F. Kavehmadavani, V.-D. Nguyen, T. X. Vu, and S. Chatzinotas, "Intelligent traffic steering in beyond 5g open ran based on lstm traffic prediction," *IEEE Trans. Wireless Commun.*, vol. 22, no. 11, 2023.
- A. B. Kihero, M. S. J. Solaija, and H. Arslan, "Inter-numerology interference for beyond 5g," *IEEE Access*, vol. 7, 2019.
- P. K. Korrai, E. Lagunas, A. Bandi, S. K. Sharma, and S. Chatzinotas, "Joint power and resource block allocation for mixed-numerology-based 5g downlink under imperfect csi," *IEEE OJCOM*, pp. 1583–1601, 2020.
- 3GPP, "NR; Physical channels and modulation," Technical specification (TS) 38.211, Dec. 2023, version 18.1.0.
- Y. Polyanskiy, H. V. Poor, and S. Verdu, "Channel Coding Rate in the Finite Blocklength Regime," *IEEE Transactions on Information Theory*, vol. 56, no. 5, pp. 2307–2359, May 2010.
- S. Schiessl, J. Gross, and H. Al-Zubaidy, "Delay analysis for wireless fading channels with finite blocklength channel coding," in *Proc. 18th ACM MSWiM*. Cancun Mexico: ACM, Nov. 2015, pp. 13–22.
- A. Beck, A. Ben-Tal, and L. Tetruashvili, "A sequential parametric convex approximation method with applications to nonconvex truss topology design problems," *J. Global Optimization*, vol. 47, pp. 29–51, May 2010.
- Nemirovski, Arkadi, "Interior point polynomial time methods in convex programming," lecture notes 42.16 (2004): 3215–3224.
- L. Bonati, R. Shirkhani, C. Fiandrino, S. Maxenti, S. D'Oro, M. Polese, and T. Melodia, "Twinning commercial network traces on experimental open ran platforms," in *Proc. MobiCom*. ACM, Dec., p. 1914–1921.
- 3GPP, "Solutions for NR to support non-terrestrial networks (NTN): Non-terrestrial networks (NTN) related RF and co-existence aspects," Technical Specification (TS) 38.863, Dec. 2023, 18.0.0.
- , "Solutions for NR to support non-terrestrial networks," Technical report (TR) 38.821, March 2023, version 16.2.0.
- H. Nguyen-Kha, V. N. Ha, E. Lagunas, S. Chatzinotas, and J. Grotz, "Seamless 5g automotive connectivity with integrated satellite terrestrial networks in c-band," in *2024 IEEE 100th VTC-Fall*, 2024, pp. 1–5.